Atmos. Chem. Phys. Discuss., 13, 27717–27777, 2013
www.atmos-chem-phys-discuss.net/13/27717/2013/
doi:10.5194/acpd-13-27717-2013

Atmospheric Chemistry and Physics Discussions

Improvement and further development in CESM/CAM5: gas-phase chemistry and inorganic aerosol treatments

J. He and Y. Zhang

Air Quality Forecasting Laboratory, Department of Marine, Earth, and Atmospheric Sciences, North Carolina State University, Raleigh, NC, 27695, USA

Received: 10 October 2013 – Accepted: 16 October 2013 – Published: 28 October 2013

Correspondence to: Y. Zhang (yang_zhang@ncsu.edu)

Published by Copernicus Publications on behalf of the European Geosciences Union.

Abstract

Gas-phase chemistry and subsequent gas-to-particle conversion processes such as new particle formation, condensation, and thermodynamic partitioning have large impacts on air quality, climate, and public health through influencing the amounts and distributions of gaseous precursors and secondary aerosols. Their roles in global air quality and climate are examined in this work using the Community Earth System Model version 1.0.5 (CESM1.0.5) with the Community Atmosphere Model version 5.1 (CAM5.1) (referred to as CESM1.0.5/CAM5.1). CAM5.1 includes a simple chemistry that is coupled with a 7-mode prognostic Modal Aerosol Model (MAM7). MAM7 includes classical homogenous nucleation (binary and ternary) and activation nucleation (empirical first-order power law) parameterizations, and a highly-simplified inorganic aerosol thermodynamics treatment that only simulates sulfate (SO_4^{2-}) and ammonium (NH_4^+). In this work, a new gas-phase chemistry mechanism based on the 2005 Carbon Bond Mechanism for Global Extension (CB05_GE) and several advanced inorganic aerosol treatments for condensation of volatile species, ion-mediated nucleation (IMN), and explicit inorganic aerosol thermodynamics have been incorporated into CESM/CAM5.1-MAM7. Comparing to the simple gas-phase chemistry, CB05_GE can predict many more gaseous species, and improve model performance for $PM_{2.5}$, PM_{10}, $PM_{2.5}$ components, and some PM gaseous precursors such as SO_2 and NH_3 in several regions, as well as aerosol optical depth (AOD) and cloud properties (e.g., cloud fraction (CF), cloud droplet number concentration (CDNC), and shortwave cloud forcing (SWCF)) on globe. The modified condensation and aqueous-phase chemistry further improves the predictions of additional variables such as HNO_3, NO_2, and O_3 in some regions, and new particle formation rate (J) and AOD over globe. IMN can improve the predictions of secondary $PM_{2.5}$ components, $PM_{2.5}$, and PM_{10} over Europe, as well as AOD and CDNC over globe. The explicit inorganic aerosol thermodynamics using ISORROPIA II improves the predictions of all major $PM_{2.5}$ components and their gaseous precursors in some regions, as well as near-surface temperature and specific

ACPD
13, 27717–27777, 2013

humidity, precipitation, downwelling shortwave radiation, SWCF, and cloud condensation nuclei at a supersaturation of 0.5 % over globe. With all the modified and new treatments, the improved model predicts that on a global average, SWCF decreases by 2.9 $W m^{-2}$, reducing the overprediction of SWCF from 7.9 % to 0.9 %. Uncertainties in emissions can explain largely the inaccurate predictions of precursor gases (e.g., SO_2, NH_3, and NO) and primary aerosols (e.g., black carbon and primary organic matter). Additional factors leading to discrepancies between model predictions and observations include uncertainties in model treatments such as dust emissions, secondary organic aerosol formation, multiple-phase chemistry, cloud microphysics, aerosol-cloud interaction, and dry and wet deposition.

1 Introduction

Atmospheric gases and aerosols play important roles in climate change due to their ability to directly or indirectly alter the Earth's radiation balance. Atmospheric chemistry determines the distribution of important oxidants and gaseous precursors for secondary air pollutants such as ozone (O_3) and fine particular matter ($PM_{2.5}$). Meanwhile, climate change can strongly influence atmospheric chemistry and air quality. Therefore, gas-phase chemistry is an important component for atmospheric and Earth system models. Different chemical reactions and kinetic parameters can lead to differences in the predictions of gases, secondary aerosols, new particle formation rate, as well as climatic variables such as cloud condensation nuclei (CCN), cloud droplet number concentration (CDNC), and radiative forcing (Faraji et al., 2008; Luecken et al., 2008; Sarwar et al., 2008; Kim et al., 2011a; Zhang et al., 2012a; Lamarque et al., 2013; Young et al., 2013; Shindell et al., 2013).

Aerosol can influence the Earth's radiative balance by directly scattering and absorbing radiation and indirectly affecting cloud properties through acting as CCN and ice nuclei (IN). Therefore, it is important to accurately simulate aerosol size distribution, chemical composition, and properties, which can determine the magnitude of aerosol

ACPD
13, 27717–27777, 2013

radiative forcing (Koloutsou-Vakakis et al., 1998). Aerosol and its influence on climate have been included in many global climate models (GCMs) such as the Community Climate System Model (CCSM) (Collins et al., 2006; Gent et al., 2010), the 5th generation of global climate model modified from European Centre for Medium-Range Weather Forecasts in Hamburg (ECHAM5) (Roeckner et al., 2003, 2006; Stier et al., 2005), and Earth system models such as the Community Earth System Model (CESM) (Ghan et al., 2012; Liu et al., 2012), the Integrated Global System Model (IGSM) (Dutkiewicz et al., 2005; Sokolov et al., 2005; Monier et al., 2013), and the Earth System Model (ESM) (Dunne et al., 2012, 2013). However, due to the complexity of aerosol microphysical processes and their interactions with cloud processes, it remains a challenge to accurately represent those properties and processes in GCMs.

Inorganic aerosols comprise 25–50 % of fine aerosol mass (Heintzenberg, 1989), which mainly includes sulfate (SO_4^{2-}), ammonium (NH_4^+), nitrate (NO_3^-), chloride (Cl^-), and sodium (Na^+). The physical and chemical properties of these aerosols have been understood reasonably well, making it possible to simulate aerosol physical and chemical processes in GCMs. Major gas-to-particle conversion processes of inorganic aerosols include condensation, nucleation, and thermodynamics. An important factor that determines the condensation of gases is the mass accommodation coefficient (α), which can be measured through laboratory experiments. To simulate aerosol condensational growth, a constant value of α is often assumed in GCMs, which is a source of uncertainty in model predictions.

Homogeneous nucleation of H_2SO_4 vapor produces new particles that can grow to form CCN. Different nucleation parameterizations are used in GCMs or global aerosol models. For example, Kulmala et al. (2006), Sihto et al. (2006), and Kuang et al. (2008) derived empirical power laws with the first- or second-order dependencies of new particle formation rates (J) on H_2SO_4 vapor concentration from observations based on cluster-activation or barrierless kinetic mechanisms, which have been used in the Community Atmosphere Model (CAM) (Wang and Penner, 2009), the Global-through-Urban Weather Research and Forecasting model with Chemistry (GU-WRF/Chem) (Zhang

ACPD
13, 27717–27777, 2013

et al., 2012), and Global Model of Aerosol Processes (GLOMAP) (Spracklen et al., 2006). An ion-mediated nucleation (IMN) model was developed to calculate J based on ambient atmospheric conditions, H_2SO_4 vapor concentrations, ionization rate, and surface area of preexisting particles. It has been used in GEOS-Chem (Yu et al., 2008, 2010), CAM (Yu et al., 2012), and GU-WRF/Chem (Zhang et al., 2012b). Different nucleation parameterizations lead to significant differences in J predictions by regional and global models (Zhang et al., 2010) and CCN/CDNC (Yu and Luo, 2009; Pierce and Adams, 2009; Kuang et al., 2009; Zhang et al., 2012b; Yu et al., 2012). Limited observations make it difficult to validate predicted J values and appropriateness of various parameterizations.

A number of thermodynamic aerosol modules have been developed to understand physical and chemical properties of inorganic aerosols. For example, EQUISOLV II (Jacobson, 1999) has been used in a one-way nested (from global to local scales) gas, aerosol, transport, radiation, general circulation, mesoscale, and ocean model (GATOR-GCMOM) (Jacobson, 2010). EQUISOLV II uses analytical equilibrium iteration and mass flux iteration to solve equilibrium problems (Jacobson, 1999), which requires relatively large computational cost. SCAPE2 is used in the California Institute of Technology (CIT) model (Meng et al., 1998). ISORROPIA (Nenes et al., 1998) has been used in several global models such as GEOS-Chem (Bey et al., 2001), the GISS Caltech (Liao et al., 2003), and the GU-WRF/Chem (Zhang et al., 2012b) and regional models such as the Community Multiscale Air Quality model (CMAQ) (Byun and Schere, 2006) and the Comprehensive Air Quality Model with Extensions (CAMx) (ENVIRON, 2010). An updated version, ISORROPIA II (Fountoukis and Nenes, 2007), has also been implemented in recent versions of CMAQ (e.g., CMAQ v4.7-Dust (Wang et al., 2012) and CMAQ v5.0 (Appel et al., 2013)), GEOS-Chem (Fountoukis and Nenes, 2007), and ECHAM5 with MESSy Atmospheric Chemistry and Global Modal-aerosol eXtension (EMAC/GMXe) (Metzger et al., 2011). The Multicomponent Equilibrium Solver for Aerosols (MESA) (Zaveri et al., 2005) has been used in the mesoscale WRF/Chem (Fast et al., 2006). The Equilibrium Simplified Aerosol Model (EQSAM)

ACPD
13, 27717–27777, 2013

has been updated in EMAC/GMXe in the past decade (Metzger et al., 2002, 2007, and 2011). Different aerosol thermodynamic models can lead to different aerosol predictions (Nenes et al., 1998; Zhang et al., 2000; Zaveri et al., 2005; Metzger et al., 2011). Zhang et al. (2000) reported average absolute differences of 7.7–12.3 % in total PM predictions between different thermodynamic modules under 400 test conditions but the differences could be as large as 68 % under some cases (e.g., high nitrate/chloride concentrations and low/medium relative humidity (RH)). Fountoukis and Nenes (2007) found the largest discrepancies between ISORROPIA II and SCAPE2 in water concentration predictions exist under low RH conditions (RH < 60 %), primarily from differences in the treatment of water uptake and solid state composition. The 3-D atmospheric models with these modules include explicit thermodynamic treatments for sulfate, ammonium, nitrate, sodium, and chloride. For comparison, some GCMs, such as CAM, use highly-simplified thermodynamics that treats sulfate and ammonium only. Most thermodynamic modules assume thermodynamic equilibrium between the gas and particulate phases for volatile compounds. However, if the time needed for the system achieving chemical equilibrium is much longer than the time step used in the model, the equilibrium assumption is not valid, which often occurs for coarse particles and cooler conditions (Wexler and Seinfeld, 1991; Meng and Seinfeld, 1996). Therefore, it remains a challenge to simulate thermodynamics for coarse particles.

In this work, a comprehensive gas-phase chemical mechanism and detailed inorganic aerosol treatments for nucleation and aerosol thermodynamics are incorporated into CAM version 5.1 (CAM5.1) in the CESM version 1.0.5 (CESM1.0.5). Several modifications are also made to the existing treatments such as condensation and aqueous-phase chemistry. The objectives are to improve the representations of gas-phase chemistry and inorganic aerosol treatments in CESM/CAM5.1, and reduce uncertainties in the chemical and radiative predictions associated with those processes. The improved model with enhanced capabilities can be applied for decadal simulations to study interactions among atmospheric chemistry, aerosols, and climate change.

ACPD
13, 27717–27777, 2013

2 Model development and improvement

CESM is a fully-coupled global Earth system model, which includes land, ocean, atmosphere, and sea ice components. The atmosphere component used in this study is CAM5.1. Existing and new model treatments related to this study are described in this section. Further details on CAM5.1 can be found at http://www.cesm.ucar.edu/models/cesm1.0/cam/.

2.1 Existing gas-phase chemistry and aerosol treatments in CESM/CAM5.1

CAM5.1 uses a simple gas-phase chemistry for sulfur species, which includes 1 photolysis reaction and 7 kinetic reactions among 6 gas-phase species (i.e., Hydrogen peroxide (H_2O_2), sulfuric acid (H_2SO_4), sulfur dioxide (SO_2), dimethylsulfide (DMS), Ammonia (NH_3), and semi-volatile organic gas (SOAG)). A more comprehensive gas-phase mechanism with 40 photolytic reactions and 172 kinetic reactions among 103 species, i.e., the Model of OZone and Related chemical Tracers version 4 (MOZART-4) of Emmons et al. (2010), has been incorporated into the official released CAM5.1. It is, however, only coupled with the bulk aerosol module (BAM) in CAM5.1. In addition to BAM, CAM5.1 contains the modal aerosol model (MAM) that is based on modal representations of aerosols. In this study, MAM is used because it can represent more accurate size distributions as compared to BAM. There are two versions of MAM, one with seven lognormal modes (MAM7), and the other with three lognormal modes (MAM3) (Liu, et al., 2012), and both are coupled with the simple gas-phase chemistry in the default model. MAM7 is used in this study because it contains explicit treatments for ammonium and size distributions for dust, sea-salt, and primary carbon compared to MAM3. MAM7 explicitly treats sulfate, ammonium, sea-salt, dust, black carbon (BC), primary organic matter (POM), and secondary organic aerosols (SOA). It simulates condensational growth of aerosol, nucleation, coagulation, dry deposition, wet removal, and water uptake. MAM7 treats H_2SO_4, NH_3, and methanesulfonic acids (MSA) as completely non-volatile species and treats SOAG as volatile species, using

ACPD
13, 27717–27777, 2013

a constant accommodation coefficient of 0.65 for all these condensing species based on Adams and Seinfeld (2002). There are three nucleation parameterizations in MAM7. The empirical power law of Wang and Penner (2009) (WP09) is used in the planetary boundary layer (PBL), which includes a first-order dependence on H_2SO_4 vapor with a prefactor of 1×10^{-6}. The binary H_2SO_4–H_2O homogeneous nucleation of Vehkamaki et al. (2002) (VE02) and ternary H_2SO_4–NH_3–H_2O homogeneous nucleation of Merikanto et al. (2007) (ME07) are used above PBL. MAM7 also includes simplified inorganic aerosol thermodynamics that only involves sulfate and ammonium. A more detailed description of MAM can be found in Liu et al. (2012).

2.2 New and modified model treatments implemented in this work

2.2.1 Gas-phase chemical mechanism

Highly simplified gas-phase mechanism can result in large uncertainties in the predictions of oxidants and gaseous precursors for secondary aerosols. Therefore, a new gas-phase mechanism, the 2005 Carbon Bond Mechanism for Global Extension (CB05_GE) (Karamchandani et al., 2012) has been implemented into CAM5.1 using the same chemical preprocessor as MOZART-4 (Lamarque et al., 2012) and coupled with both MAM3 and MAM7. CB05_GE was developed to simulate major chemical reactions for global-through-urban applications as illustrated in Zhang et al. (2012b). A more detailed description of CB05_GE can be found in Karamchandani et al. (2012). In this study, gas precursors for SOA in CB05_GE are mapped to SOAG to make it compatible in MAM7. As the first study of CESM/CAM5.1 with CB05_GE, this work focuses on the impact of gas-phase chemistry. The heterogeneous chemistry on the surface of aerosol is turned off. CB05_GE implemented in CESM/CAM5 contains a total of 273 reactions including 50 photolysis reactions and 223 kinetic reactions among 93 gas-phase species in this study.

ACPD
13, 27717–27777, 2013

2.2.2 Ion-mediated nucleation parameterization

Ions generated by cosmic radiation and natural radioactive decay have been studied for a long time as an important source to enhance nucleation (Raes et al., 1986). An IMN model is developed by Yu (2010) (Yu10) for H_2SO_4–H_2O system, and explicitly solves the dynamic equations in terms of temperature, relative humidity, H_2SO_4 vapor concentration, ionization rate, and surface area of preexisting particles. Different from classic binary nucleation theory, which is based on the minimization of changes in Gibbs free energy (Seinfeld and Pandis, 2006), IMN is based on a kinetic model that considers the interactions among ions, neutral and charged clusters, vapor molecules, and preexisting particles (Yu and Turco, 2000, 2001; Yu, 2006, 2010). The global ionization rates due to cosmic rays are calculated based on the schemes given in Usoskin and Kovaltsov (2006) and the contribution of radioactive materials from soil to ionization rates is parameterized based on the profiles given in Reiter (1992). To reduce the computing cost using IMN in 3-D models, Yu et al. (2008) developed lookup tables with simple interpolation subroutines to calculate nucleation rates under typical atmospheric conditions. In this work, IMN based on YU10 is implemented into MAM7 and combined with default nucleation parameterizations (VE02, ME07, and WP09) in order to improve the J predictions and aerosol number concentrations in upper troposphere. The J value above PBL is taken as the maximum value among predictions from IMN (YU10) and homogeneous nucleation (VE02 or ME07), and the J value within PBL is taken as the maximum value among predictions from IMN (YU10), homogeneous nucleation (VE02 or ME07), and the first-order parameterization (WP09).

2.2.3 Inorganic aerosol thermodynamics

Gas-particle partitioning is an important process in the formation and evolution of secondary aerosols. Several factors affect gas-particle partitioning, such as temperature, relative humidity, saturation vapor pressures of species, the physical state of the condensed-phase, and the way in which aerosol components interact each other

ACPD
13, 27717–27777, 2013

(Cappa et al., 2008; Zuend et al., 2010). Most models focus on inorganic aerosols. Fountoukis and Nenes (2007) developed a computationally-efficient thermodynamics equilibrium model, ISORROPIA II, for the magnesium (Mg^{2+})-potassium (K^+)-calcium (Ca^{2+})-NH_4^+–Na^+–SO_4^{2-}–NO_3^-–Cl^-–H_2O aerosol system. An important difference between ISORROPIA II and most other thermodynamics equilibrium models is that ISORROPIA II simulates crustal species, such as Mg^{2+}, K^+, and Ca^{2+}, which are important constituents of atmospheric aerosols, in particular, mineral dust. Therefore, to explicitly simulate aerosol thermodynamics, ISORROPIA II has been implemented into MAM7 and applied for accumulation, Aitken, fine sea-salt, and fine dust modes to explicitly simulate thermodynamics of SO_4^{2-}, NH_4^+, NO_3^-, Cl^-, and Na^+ as well as the impact of crustal species associated with fine dust modes on aerosol thermodynamics. The concentrations of K^+, Ca^{2+}, and Mg^{2+} as the input for ISORROPIA II are calculated from dust concentrations, using the mass ratios of 1.022×10^{-3}, 1.701×10^{-3}, and 7.084×10^{-4}, respectively (Van Pelt and Zobeck, 2007). Aerosol thermodynamics involving coarse particles (in coarse sea-salt and coarse dust modes) is currently not treated in this work, given their non-equilibrium nature and the high computational cost for solving the non-equilibrium system involving coarse particles.

2.2.4 Modifications of existing aerosol treatments

MAM 7 does not treat NO_3^- and it treats NaCl as one species. In this work, MAM7 is modified to explicitly simulate NO_3^-, Cl^-, and Na^+. NO_3^- and Cl^- are simulated in all modes except for primary carbon mode. Na^+ is simulated in sea-salt modes. The source of Na^+ is calculated based on the mass ratio of Na and Cl from sea-salt emissions. The source of Cl^- includes sea-salt emissions, and the condensation of HCl. Species-dependent accommodation coefficients are used for H_2SO_4, NH_3, HNO_3, and HCl, with the values of 0.02, 0.097, 0.0024, and 0.005 (Zhang et al., 1998; Sander et al., 2002), respectively. Dissolution and dissociation of HNO_3 and HCl to produce

ACPD
13, 27717–27777, 2013

NO_3^- and Cl^- in cloud water are added in the model based on Schwartz (1984), Marsh and McElroy (1985), and Seinfeld and Pandis (2006).

3 Model configurations and evaluation protocols

3.1 Model setup and simulation design

Table 1 summarizes the CESM/CAM5.1 simulations that are designed to examine the impacts of individual new and modified treatments on model predictions. The first set of simulations includes two simulations with the same default MAM7 coupled with different gas-phase mechanisms: one uses the simple gas-phase chemistry (MAM_SIM) and one uses the CB05_GE (MAM_CB05_GE). A comparison of the two simulations provides an estimate of the impacts of gas-phase chemical mechanisms. The second set of simulations consists of four simulations that use the same CB05_GE gas-phase mechanism but with modified and new aerosol treatments individually and jointly. The first one is MAM_CON that uses an explicit treatment for NO_3^-, Cl^-, and Na^+ and species-dependent mass accommodation coefficients for condensation and that includes the aqueous-phase chemistry of HNO_3/NO_3^- and HCl/Cl^-. The second one is MAM_CON/IMN that uses the same treatments as MAM_CON but with IMN as one of the nucleation mechanisms and a prefactor of 1.0×10^{-8} in WP09. The third one is MAM_CON/ISO that uses the same treatments as MAM_CON but with ISORROPIA II for aerosol thermodynamics. The fourth one is MAM_NEW that uses the same treatments as MAM_CON but with all new and modified aerosol treatments and a prefactor of 1.0×10^{-9} for WP09. A comparison of MAM_CB05_GE with MAM_CON indicates the impact of modified condensation and aqueous-phase chemistry. A comparison of MAM_CON/IMN, MAM_CON/ISO, and MAM_NEW with MAM_CON indicates the impacts of IMN, ISORROPIA II, and combined new and modified aerosol treatments, respectively. The 3rd set of simulation includes one simulation using the same configuration as MAM_NEW but with adjusted emissions (MAM_NEW/EMIS). Its compar-

ACPD
13, 27717–27777, 2013

ison with MAM_NEW indicates the impacts of uncertainties in emissions on model predictions. All these simulations use the same aqueous-phase chemistry of Barth et al. (2000) and the same physical options as those in MAM_SIM. Major physical options include the cloud microphysics parameterization of Morrison and Gettelman (2008), the moisture PBL scheme of Bretherton and Park (2009a), the shallow convection scheme and deep convection scheme of Park and Bretherton (2009) and Zhang and McFarlane (1995), respectively, the aerosol activation parameterization of Abdul-Razzak and Ghan (2000), and the Rapid Radiative Transfer Model for GCMs (RRTMG) of Mlawer et al. (1997) and Iacono et al. (2003, 2008) for long and short-wave radiation. The land surface processes are simulated by the Community Land Model (CLM) of Lawrence et al. (2011) in CESM that is coupled with CAM5.1.

All simulations are performed with fully-coupled CESM1.0.5 with standard B_1850-2000_CAM5_CN configuration, which represents 1850 to 2000 transient conditions and includes all active components in CESM with biogeochemistry in the land model. The simulations are conducted for the full-year of 2001 at a horizontal resolution of $0.9^{\circ} \times 1.25^{\circ}$ and a vertical resolution of 30 layers for CAM5.1. The initial meteorological conditions are generated through the CESM framework from B_1850-2000_CAM5_CN component set. The initial chemical conditions are based on the default setting in MOZART for chemical species treated in MOZART and clean conditions for other species that are not treated in MOZART. The model is spin up for one year to generate initial conditions for the missing species. The offline anthropogenic emissions used in all simulations except for MAM_NEW/EMIS are taken from Zhang et al. (2012b). Anthropogenic emissions used in MAM_NEW/EMIS are adjusted emissions based on those of Zhang et al. (2012b), with adjustment factors of 0.7, 0.5, and 1.2 for SO_2 over CONUS, Europe, and Asia, respectively, and 1.2 for NH_3, BC, and organic carbon (OC), and 1.3 for carbon monoxide (CO) over all three regions. Those emissions are adjusted based on the comparison with the emission inventories from the Representative Concentration Pathways (RCPs), the MOZART version 4 (MOZART-4), the Reanalysis of the TROpospheric chemical composition (RETRO), the Global Fire Emis-

ACPD
13, 27717–27777, 2013

sions Database (GFED) version 2, and preliminary evaluation of CESM/CAM5.1 with modified and new gas and aerosol treatments using available observations. The online emissions include biogenic volatile organic carbon (Guenther et al., 2006), mineral dust (Zender et al., 2003), and sea-salt (Martensson et al., 2003).

3.2 Available measurements for model validation

A number of observational datasets from surface networks and satellites are used for model evaluation. They are summarized along with the variables to be evaluated in Table 2. Global surface networks include the National Climatic Data Center (NCDC), the Global Precipitation Climatology Project (GPCP), the Baseline Surface Radiation Network (BSRN), and the National Oceanic and Atmospheric Administration Climate Diagnostics Center (NOAA/CDC). The satellite datasets include the Moderate Resolution Imaging Spectroradiometer (MODIS), the Clouds and Earth's Radiant Energy System (CERES), the Total Ozone Mapping Spectrometer/the Solar Backscatter Ultra-Violet (TOMS/SBUV), the Measurements Of Pollution In The Troposphere (MOPITT), and the Global Ozone Monitoring Experiment (GOME). Other satellite-based data include the MODIS-derived CDNC from Bennartz (2007) (BE07).

Regional observational networks include the Clean Air Status and Trends Network (CASTNET), the Interagency Monitoring of Protected Visual Environments (IMPROVE), and the Speciation Trends Network (STN) over CONUS; the European Monitoring and Evaluation Program (EMEP), the Base de Données sur la Qualité de l'Air (BDQA), and the European air quality database (AirBase) over Europe; the Ministry of Environmental Protection of China (MEP of China), the National Institute for Environmental Studies of Japan (NIES of Japan), and Taiwan Air Quality Monitoring Network (TAQMN) over East Asia. The observational data of J is compiled from Kulmala et al. (2004) and Yu et al. (2008), which include land-, ship-, and aircraft-based measurements.

ACPD
13, 27717–27777, 2013

3.3 Evaluation protocol

The protocols for performance evaluation include spatial distributions and statistics, following the approach of Zhang et al. (2012b). The analysis of the performance statistics will focus on mean bias (MB) and normalized mean bias (NMB). The meteorological and radiative variables are evaluated annually, including temperature at 2 m (T2), specific humidity at 2 m (Q2), and wind speed at 10 m (WS10) from NCDC; total daily precipitation rate (Precip) from GPCP; downwelling shortwave radiation (SWD) and downwelling longwave radiation (LWD) from BSRN; outgoing longwave radiation (OLR) from NOAA/CDC; shortwave cloud forcing (SWCF) from CERES; cloud fraction (CF), aerosol optical depth (AOD), cloud optical thickness (COT), cloud water path (CWP), precipitating water vapor (PWV), and CCN from MODIS; as well as CDNC from BE07. Chemical concentrations evaluated include seasonal and annual averaged surface mixing ratios of CO, O_3, SO_2, NH_3, NO_2, and HNO_3, surface concentrations of PM and its major components (i.e., SO_4^{2-}, NO_3^-, NH_4^+, Cl^-, BC, OC, total carbon (TC)) for CONUS, Europe, and East Asia, and column tropospheric CO and NO_2, and tropospheric O_3 residual (TOR) for the globe.

4 Model evaluation for MAM_SIM based on original model treatments

Tables 3 and 4 show MBs and NMBs of meteorological/radiative and chemical predictions, respectively. The model performance of the baseline simulation, MAM_SIM, is discussed below. That for all other simulations will be discussed in Sect. 5.

As shown in Table 3, meteorological variables such as T2, Q2, and WS10 are underpredicted by 1.4 °C (~ −10.9 %), 4.3×10^{-4} g kg^{-1} (~ −5.1 %), and 0.6 m s^{-1} (~ −15.2 %), respectively, whereas Precip is overpredicted by 0.3 mm day^{-1} (~ 12.9 %). Radiative variables such as LWD and SWD are underpredicted by 3.4 W m^{-2} (~ −1.1 %) and 2.0 W m^{-2} (~ −1.1 %), respectively, whereas OLR and SWCF are overpredicted by 8.8 W m^{-2} (~ 4.1 %) and 3.2 W m^{-2} (~ 7.9 %) respectively. Cloud variables

ACPD
13, 27717–27777, 2013

such as CF and PWV are slightly underpredicted, whereas COT, CWP, column CCN at a supersaturation of 0.5 %, and CDNC are largely underpredicted, with NMBs of −77.8 % to −55.6 %, which is likely due to the limitations in the current model treatments of cloud microphysics and aerosol-cloud interactions in CAM5.1.

AOD is also underpredicted by 36.1 %, which is likely due to inaccurate predictions of aerosol concentrations. For example, as shown in Table 4, $PM_{2.5}$ concentrations over CONUS and Europe, and PM_{10} concentrations over CONUS, Europe, and East Asia are underpredicted, with NMBs of −67.5 % to −31.8 %, which is due to the inaccurate predictions of SO_4^{2-}, NH_4^+, and organic aerosols, and missing major inorganic aerosol species such as nitrate and chloride. The concentrations of BC, OC, and TC are underpredicted (by ∼ 50 %), which is likely due to the uncertainties in the BC and primary OC emissions as well as treatments for SOA formation. In particular, the SOA treatment used in CAM5.1 is based on a highly-simplified aerosol yield approach with a single lumped semi-volatile organic gas (i.e., SOAG). For gaseous species, SO_2 concentrations over CONUS and Europe are significantly overpredicted by 10.3 $\mu g\,m^{-3}$ (∼ 264.8 %) and 6.6 $\mu g\,m^{-3}$ (∼ 97.5 %), respectively, whereas SO_2 concentrations over East Asia are largely underpredicted by 7.9 $\mu g\,m^{-3}$ (∼ 63.0 %). NH_3 concentrations over Europe are also largely underpredicted by 82.0 %. These large biases in SO_2 and NH_3 are likely due in part to the uncertainties in the emissions of SO_2 and NH_3, which in turn affect the predictions of SO_4^{2-} and NH_4^+. The J values in PBL are highly underpredicted by 99.6 %, which is mainly due to the inaccurate calculation of H_2SO_4 vapor concentration that participates in the nucleation and uncertainties in the nucleation parameterizations used in the default CESM/CAM5.1.

ACPD
13, 27717–27777, 2013

5 Impacts of new and modified treatments on model predictions

5.1 Impacts of new gas-phase chemistry

Compared to simple gas-phase chemistry, many more gaseous species and chemical reactions simulated in CB05_GE can affect secondary aerosol formation through gas-to-particle mass transfer and aqueous-phase chemistry and affect meteorological/climatic variables through chemistry feedbacks to the climate system. Figure 1 shows the absolute differences of T2, WS10, PBL height (PBLH), H_2O_2, SO_2, SO_4^{2-}, SOA, sea-salt (SSLT), and dust (DUST) between MAM_CB05_GE and MAM_SIM. Compared to MAM_SIM, MAM_CB05_GE predicts higher global average T2 and WS10, but lower PBLH, due to various feedbacks to meteorology caused by changed chemical concentrations, although the directions of such changes are region-dependent. For example, T2 increases by up to 4 °C over most areas in Asia, but decreases over most areas by as large as 4.1 °C in North America. PBLH simulated by MAM_CB05_GE is lower than that by MAM_SIM by as much as 312.6 m, or higher by as much as 176.5 m. There are strong correlations in changes in related variables. For example, the increase of T2 over land in the Northern Hemisphere is mainly due to the combined effects of increase of SWD from decreased CF and increase of latent heat flux (Figure not shown) in the same regions; and the decrease of T2 in the Northern Hemisphere and the decrease of T2 over land in the Southern Hemisphere are mainly due to the decrease of SWD, resulting from an increase in CF. The changes in meteorological/radiative variables in turn affect chemical predictions during subsequent time steps. For example, the change of T2 can in turn affect the rates of temperature-dependent chemical reactions.

MAM_CB05_GE treats more gaseous species and chemical reactions than MAM_SIM, leading to large changes in the concentrations of gaseous and PM species. Compared with MAM_SIM, MAM_CB05_GE predicts higher H_2O_2 by 0.4 ppb, SO_2 by 7.3 ppt, SO_4^{2-} by 0.01 $\mu g\,m^{-3}$, and SOA by 0.06 $\mu g\,m^{-3}$ in terms of global mean.

ACPD
13, 27717–27777, 2013

Those changes are mainly caused by different gas-phase chemical mechanisms used in MAM_SIM and MAM_CB05_GE. While MAM_CB05_GE explicitly simulates O_3 and OH radicals, O_3 chemistry is not treated and OH is prescribed in MAM_SIM in default CESM/CAM5.1. OH simulated by MAM_CB05_GE is lower than that prescribed by MAM_SIM by up to 0.12 ppt, or higher by up to 0.12 ppt in different regions (Figure not shown), with a higher global mean by MAM_CB05_GE. MAM_SIM includes the production of H_2O_2 from the self-destruction of HO_2 and the loss of H_2O_2 through its photolytic reaction and its reaction with OH. Higher H_2O_2 in MAM_CB05_GE is mainly due to greater production of H_2O_2 from additional chemical reactions (e.g., OH + OH) than loss of H_2O_2 through the reactions of OH + H_2O_2, O + H_2O_2, Cl + H_2O_2, and Hg + H_2O_2. Different predictions in H_2O_2 can in turn affect OH mixing ratios in MAM_CB05_GE but not in MAM_SIM. In addition, the photolytic reactions of VOCs (e.g., HCHO, peroxyacyl nitrates (PAN), and peroxyacetic and higher peroxycarboxylic acids (PACD)) and other gases (e.g., HNO_3, HONO, HNO_4, HOCl, and HOBr) treated in MAM_CB05_GE can produce OH. Despite higher OH mixing ratios in MAM_CB05_GE, many gaseous species such as NO_x, SO_2, HNO_3, HONO, and other VOCs are oxidized by OH to form secondary inorganic and organic aerosols. Those oxidation reactions compete for limited OH, leading to less oxidation of SO_2, thus higher SO_2 mixing ratios over most land areas by MAM_CB05_GE. Lower SO_2 mixing ratios over the oceanic areas in MAM_CB05_GE is due to the combined effects of less production of SO_2 from lower DMS mixing ratios (due to increased PBLH and OH levels) and greater SO_2 oxidation from higher OH mixing ratios.

The changes in the concentrations of PM and its components are due to the change in the mixing ratios of gaseous precursors and meteorological conditions. CB05_GE contains more photolytic reactions, which affect the mixing ratios of OH, SO_2, and H_2SO_4, and subsequently the concentration of SO_4^{2-} through condensation and homogeneous nucleation. Higher SO_2 mixing ratios in MAM_CB05_GE result in more H_2SO_4 thus more SO_4^{2-}. For example, both SO_2 mixing ratios and SO_4^{2-} concentrations are higher over eastern China in MAM_CB05_GE. T2 is higher, resulting in more

ACPD
13, 27717–27777, 2013

SO_4^{2-} from SO_2 oxidation and WS10 is lower, resulting in more SO_4^{2-} near surface. More SO_4^{2-} over the oceanic areas is mainly due to more oxidation of SO_2 by OH. Due to the simplification of aerosol thermodynamics in default MAM7, the concentrations of SO_4^{2-} can affect the concentrations of NH_4^+ directly and therefore NH_3 mixing ratios and PM number concentrations (PM_{num}). For example, the increase of SO_4^{2-} results in an increase in NH_4^+ and PM_{num}, and a decrease in NH_3. The increase of SO_4^{2-} and PM_{num} can increase AOD, CF, COT, CWP, PWV, and CDNC and therefore affect radiation by increasing LWD and decreasing SWD (Figures not shown, see changes in performance statistics of these affected variables in Table 3). The increase of SOA is due to the inclusion of more gaseous precursor emissions (e.g., isoprene, terpene, xylene, and toluene) in MAM_CB05_GE, which contribute to SOAG and thus SOA through gas-to-particle conversion.

Unlike gases and secondary aerosol species, the changes of sea-salt and dust concentrations are mainly attributed to the change of WS10. A small change of WS10 can result in a significant change of sea-salt and dust emissions, and thus $PM_{2.5}$ and PM_{10}. This can be reflected by a strong correlation between spatial patterns of WS10 and sea-salt, and between the same directional changes in WS10 and dust concentrations over major deserts such as Gobi and Takla Makan deserts where the dust concentrations decrease with lower WS10, and Arabian and Sahara/Sahel deserts where the dust concentrations increase with higher WS10. However, the changes in dust concentrations are the opposite to those in WS10 in some regions. For example, dust emissions increase with the decreased WS10 in some regions such as arid regions in Russia, Mongolia, and most northern China and decrease with increased WS10 over some regions such as Australia. Such an anti-correlation indicates the influences on dust emissions and concentrations by factors other than WS10. For example, changes in precipitation can affect lifetime of dust particles in the atmosphere through wet scavenging. The decreased (or increased) wet deposition of dust resulted from decreased (or increased) precipitation in those regions (Figure not shown).

ACPD
13, 27717–27777, 2013

Figure 2 shows the spatial distributions of CO, O_3, NO_2, HNO_3, hydrochloric acid (HCl), and isoprene (ISOP) that can be predicted by MAM_CB05_GE but not by MAM_SIM. CO mixing ratios are higher in most Asia, central Africa, South Africa, and eastern US, which is mainly due to higher CO emissions in those regions and the production of CO from the photolytic reactions of VOCs (e.g., formaldehyde, acetaldehyde, and isoprene). Higher O_3 mixing ratios in the Northern Hemisphere than Southern Hemisphere are mainly due to much higher mixing ratios of O_3 precursors. Higher O_3 mixing ratios over Mediterranean Sea are mainly due to the transport of O_3 and its precursors from source regions and less deposition onto ocean surface. Higher O_3 mixing ratios over Tibet are mainly due to the stratospheric influences from high altitude and no titration of O_3 due to low NO mixing ratios (< 0.2 ppb) in this region. Higher mixing ratios of NO_2 over most Asia, eastern U.S, Europe, and Central Africa are mainly due to higher NO_x emissions over those regions, which also result in higher HNO_3 in those regions. Higher mixing ratios of HCl over Europe, India, and East Asia are mainly due to the higher anthropogenic HCl emissions in those regions. In addition, MAM_CB05_GE includes oceanic emissions of HCl, leading to higher HCl over ocean. Higher isoprene mixing ratios over South Africa, central Africa, and Oceania are mainly due to higher isoprene emissions in those regions, which also contribute to the formation of SOA in those regions.

The aforementioned changes in the concentrations of gaseous species and PM result in a change in predicted cloud properties and radiation balance that in turn affect the predictions of other meteorological variables such as T2 and WS10 and all chemical species during subsequent time steps. As a consequence of interwoven changes due to complex feedback mechanisms, the two simulations perform differently, with noticeable improvement by MAM_CB05_GE. As shown in Table 3, compared with MAM_SIM, MAM_CB05_GE reduces MB of Q2 by 18.6 %, LWD by 17.6 %, OLR by 8.0 %, CF by 28.6 %, COT by 1.0 %, PWV by 28.0 %, AOD by 5.5 %, and CDNC by 1.8 %, leading to 0.3–2.2 % absolute reduction in their NMBs. Although MAM_CB05_GE increases MB of T2 by 7.1 %, WS10 by 3.4 %, and SWD by 26.2 %, the increases in their NMBs

ACPD
13, 27717–27777, 2013

are only 0.2–1.2 %. As shown in Table 4, MAM_CB05_GE also reduces MBs of SO_2 by 2.5 % and PM_{10} by 8.1 % over East Asia, NH_3 by 1.3 % and SO_4^{2-} by 12.5 % over Europe, OC by 11.1 %, TC by 8.3 %, and $PM_{2.5}$ by 3.3 % over CONUS, leading to 0.8–6.5 % absolute reductions in NMBs. Despite the model improvement by CB05_GE, large biases still remain for some chemical species. For example, CO over East Asia is largely underpredicted with an NMB of −82.1 % (see Table 4), which results from the uncertainties in the CO emissions over East Asia. However, the column CO over globe is predicted very well, with an NMB of −5.7 %. Large biases in SO_2 predictions over CONUS, Europe, and East Asia are mainly due to the uncertainties in the SO_2 emissions over those regions. Large biases in O_3 over Europe are likely due to the uncertainties in the O_3 precursor emissions (e.g., NO_x) and inaccurate predictions of meteorology and radiation over Europe. In particular, the large underpredictions in NO_2 concentrations (likely due to the uncertainties in the NO_x emissions and overpredictions in radiation, see Sect. 5.5 for more detailed discussions) indicate insufficient NO_x for titration of O_3, leading to a large overprediction in O_3 concentrations in Europe. The large biases in HNO_3 are due to no treatment for gas-particle partitioning in both simulations.

5.2 Impacts of condensation and aqueous-phase chemistry

The α value for H_2SO_4 vapor is subject to considerable uncertainty. The calculation in the default condensation module with a default α value of 0.65 gives a very low concentration of H_2SO_4, resulting in very low nucleation rates and aerosol number concentrations. Considering that the original model treats H_2SO_4 and NH_3 condensation as an irreversible process, the default α value of 0.65 for H_2SO_4 and NH_3 is reduced to 0.02 and 0.097, respectively, based on Zhang et al. (1998). This change in α value provides sufficient H_2SO_4 and NH_3 for nucleation with a typical H_2SO_4 concentration range of $10^6 \sim 10^8$ molecules cm^{-3}. Because HNO_3 and HCl are semi-volatile species, the lower limits of α (0.0024 and 0.005, respectively) based on Sander et al. (2002)

ACPD
13, 27717–27777, 2013

are selected for their irreversible condensation process. NH_4^+ from NH_3 condensation will be constrained by the available SO_4^{2-}, NO_3^-, and condensed Cl^-, following the approach that is used in the default simplified thermodynamics to neutralize the cations in the system.

Figure 3 shows the absolute differences of NH_3, SO_2, HNO_3, HCl, H_2SO_4, total particulate ammonium (TNH_4), total particulate sulfate (TSO_4), total particulate nitrate (TNO_3), and total particulate chloride (TCL) in all the modes except primary carbon mode, and $PM_{2.5}$ between MAM_CON and MAM_CB05_GE in June, July, and August (JJA), 2001. Due to the inclusion of HNO_3 and HCl condensation in MAM_CON, the concentrations of HNO_3 and HCl decrease by 0.1 ppb (~ 72 %) and 0.097 ppb (~ 84 %), respectively. NO_3^- is not simulated in the original model and the concentration of NO_3^- is assumed as zero in MAM_CB05_GE. Therefore, the concentration of NO_3^- increases due to the condensation of HNO_3 in MAM_CON. The concentration of TCL in MAM_CB05_GE is calculated from the mass ratio of chloride in sea-salt. Over land, TCL increases significantly due to the condensation of HCl to form Cl^-. The change of TCL over ocean is mainly due to the change of WS10, which has a significant impact on sea-salt emissions. The changes of SO_2 mixing ratios are mainly due to the differences in meteorology and mixing ratios of species in sulfur chemistry in the two simulations. For example, compared to MAM_CB05_GE, PBLH (Figure not shown) in MAM_CON either increases by up to 394.3 m or decreases by up to 392.1 m, which can affect vertical mixing and SO_2 mixing ratios near the surface. The increase of SO_2 over eastern US is likely due to the less SO_2 oxidation in clouds (Figure not shown), which results from lower CF. However, for those regions that both SO_2 and CF increase (e.g., North Russia and East Asia), the increase of SO_2 is likely due to the decrease of PBLH. The decrease of SO_2 mixing ratios over most oceanic areas is likely due to the combined effects of DMS oxidation and SO_2 oxidations in MAM_CON. More SO_2 can result in more H_2SO_4 and therefore more SO_4^{2-} through condensation and homogeneous nucleation of H_2SO_4. The changes in H_2SO_4 concentrations are the results of changes of SO_2 mixing ratios. The mass accommodation coefficient of H_2SO_4 is reduced significantly

ACPD
13, 27717–27777, 2013

(by a factor of 32.5), allowing more H_2SO_4 to participate in binary/ternary homogeneous nucleation and produce more secondary SO_4^{2-}, improving predictions of SO_4^{2-} over CONUS but degrading the performance of SO_4^{2-} over Europe (see Table 4). Although the mass accommodation coefficient of NH_3 is reduced significantly (by a factor of 67), more available NH_3 can participate in the ternary homogeneous nucleation and produce secondary NH_4^+. Meanwhile, the secondary NH_4^+ formed from NH_3 condensation is also constrained by available SO_4^{2-}, NO_3^-, and condensed Cl^-. As a result, NH_3 mixing ratios decrease and NH_4^+ concentrations increase. Due to more available H_2SO_4 participating in the nucleation, J has been improved significantly, reducing the NMB from −99.5 % to −12.8 %. With an inclusion of the dissolution and dissociation of HNO_3 and HCl in cloud water, more NH_3 is required to dissolve to maintain cation-anion equilibrium in the cloud water, which further reduces the mixing ratios of NH_3, HNO_3, and HCl.

As shown in Table 4, compared with MAM_CB05_GE, MAM_CON gives better performance against observations in terms of CO, NO_2, O_3, HNO_3, $PM_{2.5}$, and PM_{10} over Europe, CO and PM_{10} over East Asia, O_3, HNO_3, SO_4^{2-}, NH_4^+, BC, OC, TC, and $PM_{2.5}$ over CONUS, and column CO, column NO_2, TOR, and J over globe. As also shown in Table 3, the improved chemical predictions improve the predictions of WS10, Precip, OLR, SWCF, CF, COT, CWP, AOD, and CDNC. Treating condensation and aqueous-phase chemistry of HNO_3 and HCl enables an explicit simulation of NO_3^- and Cl^- in MAM7. However, the mass concentrations of SO_2 remain significant overpredictions, with NMBs of 301.2 % for CONUS, and 123.0 % for Europe, mainly because of the uncertainties in SO_2 emissions over those regions. Due to the simplified irreversible treatment for gas condensation, the mass concentrations of SO_4^{2-}, NH_4^+, NO_3^-, and Cl^- are overpredicted, although the lower limit of mass accommodation coefficient for each precursor is used in MAM_CON. As shown in Table 4, the concentrations of SO_4^{2-}, NH_4^+, NO_3^-, and Cl^- from MAM_CON are overpredicted by 1.7 %, 20.0 %, 198.2 %, and 359.9 %, respectively, for CONUS, and 40.3 %, 85.0 %, 67.8 %, and 102.8 %, respec-

ACPD
13, 27717–27777, 2013

tively, for Europe. The large NMBs of NO_3^- and Cl^- in MAM_CON are due to the small observed values for NO_3^- (i.e., 1.0 μg m^{-3} over CONUS and 2.0 μg m^{-3} over Europe) and Cl^- (i.e., 0.1 μg m^{-3} over CONUS and 0.7 μg m^{-3} over Europe), the uncertainties in treating HNO_3 and HCl as non-volatile species using their lower limits of accommodation coefficients, and lack of treatments for NO_3^- and Cl^- thermodynamics.

5.3 Impacts of new particle formation

Figure 4 shows the annual-mean vertical distributions of J values and aerosol number concentrations, and simulated J values averaged between the ground level and 1000 m overlaid with observations within the same layers. In MAM_CON/IMN, IMN is combined with three default nucleation parameterizations to predict J throughout the atmosphere. In MAM_CON, J over ocean is overpredicted by factors of 5–50, despite a seeming good NMB of −12.8 % in the globe mean (see Table 4). J values at several sites over land are underpredicted by factors of 1–10, which compensates the large overpredictions at most sites over ocean. The large underpredictions at those sites are likely due to the uncertainties in SO_2 emissions and nucleation parameterizations, and the missing species that may have participated in nucleation. For example, several other species may contribute to the new particle formation, including methanesulfonic acid (van Dingenen and Raes, 1993), hydrochloric acid (Arstila et al., 1999), organic compounds (Berndt, et al., 2013), iodine-containing compounds (Hoffmann et al., 2001; O'Dowd et al., 2002; Burkholder, et al., 2004; Pechtl et al., 2006), and amines (Kurtén et al., 2008; Berndt, et al., 2013). Limited observations also introduce some uncertainties in the model validation. The overprediction of J over ocean is mainly due to the use of the prefactor of 1×10^{-6} in WP09. This prefactor is derived from limited in-situ measurements (Sihto et al., 2006). It can vary by up to 3–4 orders of magnitude based on measurements in different areas and seasons (Zhang et al., 2010), introducing a large uncertainty for its application to the global scale. In MAM_CON/IMN, a prefactor of 1×10^{-8} is used in WP09 in PBL over the globe, which then decreases

ACPD
13, 27717–27777, 2013

J and aerosol number concentrations in PBL (see Fig. 4). J in PBL is very sensitive to the prefactor in WP09, and the uncertainty of the prefactor can result in a large bias in predictions of J and aerosol number in PBL. With the implementation of IMN, J values in the troposphere increase by factors of 2–10, which in turn increase the aerosol number concentrations in the troposphere. Due to a stronger radiation in the upper layer, more available ions can contribute to the new particle formation, therefore increasing the aerosol number concentrations in the middle/upper troposphere and lower stratosphere by factors of 2–4.

Figure 5 shows the absolute differences of T2, WS10, $PM_{2.5}$, AOD, column CCN at a supersaturation of 0.5 %, CF, SWCF, and SWD between MAM_CON and MAM_CON/IMN for 2001. Compared with MAM_CON, MAM_CON/IMN predicts higher global average T2 but lower WS10, due to various feedbacks to meteorology caused by changed aerosol number concentrations. Aerosol number can directly affect CCN, which can affect cloud formation and properties as well as radiation. As a result of all those changes, major PBL variables such as T2 and WS10, are changed, with global mean changes of 0.15 °C (or by 1.1 %) and 0.04 $m\,s^{-1}$ (or by 0.7 %), respectively. The decrease of T2 over Australia correlates with the increase of CF, which can decrease SWD, and the increase of T2 over land areas in the Northern Hemisphere correlates with the increase of SWD due to the decrease of CF. WS10 can affect dust and sea-salt emissions and the atmospheric transport of particles, therefore affecting $PM_{2.5}$ and PM_{10}, with a global mean changes of 0.2 $\mu g\,m^{-3}$ and 0.97 $\mu g\,m^{-3}$, respectively. Changes of PM concentrations also have impacts on AOD, CCN, CF, COT, and SWCF through both aerosol direct and indirect effects. As a net result of all those interwoven changes initially triggered by the increase of aerosol number concentrations in troposphere/stratosphere, AOD and column CCN at a supersaturation of 0.5 % increase by 0.004 (or by 3.3 %) and $2.1 \times 10^7\,cm^{-2}$ (or by 11.9 %), respectively, and SWCF and SWD decrease by 0.1 $W\,m^{-2}$ (or by 0.2 %) and 0.8 $W\,m^{-2}$ (or by 0.5 %), respectively, in terms of global mean.

ACPD
13, 27717–27777, 2013

Compared with MAM_CON, IMN (MAM_CON/IMN) improves the predictions of SO_2, NO_3^-, and $PM_{2.5}$ over CONUS, SO_2, SO_4^{2-}, NH_4^+, NO_3^-, Cl^-, $PM_{2.5}$, and PM_{10} over Europe, PM_{10} over East Asia (see Table 4). The improved performance in aerosol concentrations and increased aerosol numbers in the troposphere and lower stratosphere contribute to the improved performance of aerosol and cloud parameters, with increased AOD, CCN, and CDNC, and consequently increased CF, COT, CWP, and SWCF, as shown in Table 3. However, there are still large biases for some chemical species predictions. For example, CO mixing ratios are underpredicted over East Asia, which is mainly due to the uncertainty in CO emissions in this region. Large biases in SO_2 predictions over CONUS, Europe, and East Asia are mainly due to the uncertainties in SO_2 emissions in those regions. Large biases in NO_2 and HNO_3 predictions over Europe are mainly due to the uncertainties in NO_x emissions and inaccurate predictions of meteorology and radiation over this region. The performance of J degrades with NMBs from −21.8 % to −49.6 % in the globe, which is due to the use of a smaller prefactor of WP09 in MAM_CON/IMN than in MAM_CON. J in PBL is very sensitive to the prefactor in WP09. Although the prediction of J over ocean in PBL has been improved in MAM_CON/IMN, J over land areas in PBL is largely underpredicted by factors of 1–100, resulting in degraded J performance in terms of globe mean. The underprediction of J over land in PBL is likely due to the uncertainties in the nucleation parameterizations (e.g., the missing species as mentioned previously). Large NMBs still remain for COT, CWP, and CCN, indicating the uncertainties in the treatments of related atmospheric processes such as cloud microphysics and aerosol–cloud interactions.

5.4 Impacts of gas-aerosol partitioning

The inclusion of ISORROPIA II changes the mass concentrations of major $PM_{2.5}$ species and their gaseous precursors. Changes in PM concentrations then affect predictions of cloud variables and therefore radiation. Changes in radiation can affect predictions of meteorological variables such as PBLH. The changes in PBLH vary from

ACPD
13, 27717–27777, 2013

−245.2 m to 318.6 m, which can significantly affect gaseous and PM species in PBL. Meanwhile, changes of radiation can also affect SO_2 oxidation by OH, which affects H_2SO_4 mixing ratios. Figure 6a shows the absolute differences of H_2SO_4, fine particulate sulfate (SO4f), NH_3, fine particulate ammonium (NH4f), HNO_3, fine particulate nitrate (NO3f), HCl, and fine particulate chloride (CLf) for summer 2001 between MAM_CON and MAM_CON/ISO. Similar plots for winter (December, January, and February (DJF)) 2001 are shown in Fig. 6b. Compared to MAM_CON, MAM_CON/ISO gives higher H_2SO_4 mixing ratios but lower SO4f concentrations. SWD increases with the global mean of 8.9 $W\,m^{-2}$ (~ 5.8 %) in MAM_CON/ISO, which allows more production of OH from photolytic reactions of VOCs, HONO, HNO_3, HNO_4, H_2O_2, HOCl, and HOBr, and therefore enhanced oxidation of SO_2 to form H_2SO_4. As shown in Fig. 6a, the mixing ratios of H_2SO_4 either increase up to 0.76 ppt or decrease as large as 1.14 ppt, leading to a net increase of 0.002 ppt in terms of global mean. The mass concentration of SO4f is mainly affected by H_2SO_4 condensation. Although the mixing ratios of H_2SO_4 increase with the global mean change of 0.002 ppt, SO4f concentrations decrease with the global mean of 0.02 $\mu g\,m^{-3}$, which are mainly due to less condensation of H_2SO_4 under higher temperature conditions. In summer, the increase or decrease of H_2SO_4 can result in an increase or a decrease of SO4f (e.g., over most oceanic areas). However, the decrease of SO4f with the increase of H_2SO_4 over the India Ocean is mainly due to less H_2SO_4 condensation. For the regions where SO4f increases over land, the increase of SO4f is due to more oxidation of SO_2 by OH. For the regions where SO4f decreases over land, the decrease of SO4f is mainly due to the less H_2SO_4 condensation under higher temperature conditions. However, the decrease of SO4f over Australia is mainly due to the increased precipitation. Due to the increase of SWD, T2 has also increased by 0.2 °C, which evaporates more volatile gases, resulting in an increase in the mixing ratios of NH_3, HNO_3, and HCl, and therefore a decrease in NH_4^+, NO_3^-, and Cl^-.

Compared to MAM_CON, the mixing ratios of NH_3, HNO_3, and HCl increase significantly over most land areas, whereas NH4f, NO3f, and Clf decrease significantly

ACPD
13, 27717–27777, 2013

over most land areas in MAM_CON/ISO. The chemical regime is the controlling factor for gas-aerosol equilibrium partitioning, which is determined based on the ratio of SO_4^{2-} molar concentrations to total molar concentrations of cations and their respective gases (referred to as TCAT/TSO4) (Zhang et al., 2000). Three regimes are defined based on the values of TCAT/TSO4: (1) if TCAT/TSO4 < 2, the system contains excess sulfate and is in a sulfate-rich regime; (2) if TCAT/TSO4 = 2, the system contains just sufficient sulfate to neutralize the cation species and is in sulfate-neutral regime; (3) if TCAT/TSO4 > 2, the system contains insufficient sulfate to neutralize the cation species and is in sulfate-poor regime. Over land, the major cation is NH_4^+, and there are also crustal species (K^+, Ca^{2+}, and Mg^{2+}) associated with dust emissions, whereas over ocean, the major cation is Na^+, which is a non-volatile species. Therefore, the gas-aerosol equilibrium partitioning behaves differently over land and over ocean. Figure 7 shows the distributions of TCAT/TSO4 in MAM_CON and MAM_CON/ISO, and their absolute differences for summer and winter, 2001. In summer, compared to MAM_CON, TCAT/TSO4 in MAM_CON/ISO either increases up by 80.1 (mostly over ocean) or decreases up by 51.8 (over both land and ocean), leading to a net increase of 0.7. In MAM_CON, most regions are in sulfate-poor regime, whereas Greenland, southeast US, North Africa, a small portion of Asia and North Atlantic Ocean, and some areas in North Pole are in sulfate-rich regime in summer. However, due to the simplified thermodynamics treatment in MAM_CON, NH_3 is underpredicted and NH_4^+ is overpredicted (see Table 4). With the inclusion of ISORROPIA II, most sulfate-poor regions over land and over part of Pacific Ocean and most Atlantic Ocean become less sulfate-poor. The sulfate-poor regime can drive HNO_3/HCl to produce NO_3^-/Cl^- by neutralizing excess NH_4^+. If the amount of NO_3^-/Cl^- is insufficient to neutralize NH_4^+, sulfate-poor regime can drive NH_4^+ to the gas phase to produce NH_3. Therefore, the increase of NH_3 and decrease of NH_4^+ in MAM_CON/ISO are mainly due to insufficient NO_3^-/Cl^- to neutralize NH_4^+ under sulfate-poor regime, which results from the evaporation of NO_3^-/Cl^- to produce HNO_3 and HCl under higher temperature conditions. The slight increase of NO_3^- over Pacific Ocean and South Atlantic Ocean is due to

ACPD
13, 27717–27777, 2013

much higher Na^+ concentrations yet insufficient SO_4^{2-} in those regions compared with those over the land areas. Unlike a sulfate-poor regime, a sulfate-rich regime (e.g., small portion of North Atlantic Ocean, South China Sea, and Greenland), requires more cations such as NH_4^+ and Na^+ to neutralize excess SO_4^{2-} in the system and the thermodynamics favors the partitioning of volatile species such as NO_3^- and Cl^- in the gas phase as HNO_3 and HCl. Therefore, despite the increased temperatures, the decrease of NH_4^+ due to its evaporation back to the gas-phase is not as significant as that of NO_3^- and Cl^-, because NH_4^+ needs to stay in the system to neutralize SO_4^{2-}. In winter, as shown in Fig. 6b, compared with MAM_CON, the mixing ratios of H_2SO_4 in MAM_CON/ISO either increase by up to 4.3 ppt, or decrease by up to 1.0 ppt, leading to a net increase with the global mean of 0.001 ppt. NH_3 increases over most regions except Europe, eastern China, and some regions in North Pole. HNO_3 decreases over most oceanic areas, Northeastern China, and East Europe, whereas increases over South Asia, North Pole, southern US, Africa, and most land areas in Southern Hemisphere. HCl increases over most areas except the northeastern portion of Asia and eastern Europe.

Compared with MAM_CON, MAM_CON/ISO predicts higher T2 by 0.2 °C in winter, favoring as the presence of volatile species in the gas-phase, resulting in an increased level of HNO_3 and HCl over some land areas. As shown in Fig. 7, in MAM_CON, most regions are in sulfate-poor regime, whereas Greenland, North Pole, North Africa, some portions of Asia and western Pacific Ocean are in sulfate-rich regime. For example, northeastern China is in sulfate-poor regime, driving HNO_3 and HCl partitioning to the aerosol phase to neutralize excess NH_4^+. This results in an increase in NO3f and Clf, changing sulfate-poor regime to less sulfate-poor. North Pacific Ocean and southern oceanic areas are also in sulfate-poor regime, and the increase of NO3f is due to the partitioning HNO_3 to the aerosol phase to neutralize Na^+, whose concentration is relatively higher compared to that over land areas. Therefore, more anions such as NO_3^- are needed to neutralize the system. However, the decrease Cl^- over these regions is due to the equilibrium state of HCl under different atmospheric conditions.

ACPD
13, 27717–27777, 2013

The western Pacific Ocean is in sulfate-rich regime, driving NO_3^- and Cl^- partition to the gas phase, which results in a decrease in NO3f and Clf, and an increase in HNO_3 and HCl over this region. With the inclusion of ISORROPIA II, the western Pacific Ocean changes from sulfate-rich regime to less sulfate-rich regime.

Compared to MAM_CON, the prediction of SWD in MAM_CON/ISO is improved with the NMB decreasing from −6.5 % to −2.2 %. The predictions of involved species such as NH_4^+, NO_3^-, and Cl^- are improved significantly by 13.6 %~345.4 %, although there is a slight degradation in the predictions of SO_4^{2-} and O_3 over CONUS, CO, O_3, $PM_{2.5}$, and PM_{10} over Europe, PM_{10} over East Asia, and column CO, NO_2, TOR, and *J* over globe. MAM_CON/ISO improves the predictions of HNO_3, NH_4^+, NO_3^-, Cl^-, BC, OC, TC, and $PM_{2.5}$ over CONUS, SO_2, NH_3, NO_2, SO_4^{2-}, NH_4^+, NO_3^-, and Cl^- over Europe, and CO and SO_2 over East Asia, which leads to improved performance in T2, Q2, Precip, SWD, CCN at a superstation of 0.5 %, and SWCF over globe, as shown in Table 3. ISORROPIA II calculates gas-aerosol partitioning under different atmospheric conditions, significantly improving predictions of major gas precursor (e.g., HNO_3) over CONUS and secondary aerosols (e.g., NO_3^- and Cl^-) over CONUS and Europe. Large decreases in the concentrations of NO_3^- and Cl^- result in a decrease in NH_4^+, $PM_{2.5}$, and PM_{10}, thus decreasing CCN, CDNC, AOD, and the absolute value of SWCF.

5.5 Overall impacts of all new and modified model treatments

Figure 8 shows the absolute differences of surface SO_2, NH_3, SO_4^{2-}, NH_4^+, TC, $PM_{2.5}$, PM_{10}, *J*, and aerosol number (PM_{num}) for 2001 and Fig. 9 shows the absolute differences of radiative and meteorological variables between MAM_NEW and MAM_SIM. With the new and modified model treatments in MAM_NEW, PM and precursor gaseous species have changed significantly. Due to the aerosol direct and indirect effects, radiation and meteorology also change in MAM_NEW, which can in turn affect gas-phase chemistry such as photolytic reactions and the oxidation of SO_2 by OH. An increase of SO_2 over western Europe and northeastern US with a decrease

ACPD
13, 27717–27777, 2013

of SO_4^{2-} in those regions due to less oxidation of SO_2 under cooler conditions (see reduced T in this region in Fig. 8). On the other hand, SO_4^{2-} over East Asia increases in MAM_NEW with the increase of SO_2, causing by enhanced SO_2 oxidation under warmer conditions and reduced wet scavenging under drier conditions (see increased T and decreased Precip in this region in Fig. 8). The changes of NH_3 and NH_4^+ are due to the gas-aerosol partitioning based on ISORROPIA II. The increase in TC is due to the inclusion of more organic gases in CB05_GE, which contribute to SOAG and thus SOA. All above changes can also contribute to the changes of $PM_{2.5}$ and PM_{10}.

As shown in Fig. 8, the difference of T2 between the two simulations varies from −6.0 to 4.8 °C, with a global mean difference of about −0.1 °C. The changes of temperature can affect temperature-dependent chemical reactions and atmospheric processes, as illustrated in Fig. 7. The difference of WS10 varies from −1.5 to1.4 $m\,s^{-1}$, with a global mean of $-0.02\,m\,s^{-1}$. The decrease of wind speeds can decrease the sea-salt and dust emissions significantly and affect transport of particles as well, which can affect aerosol mass and number concentrations. Smaller prefactor 1×10^9 in WP09 is used in MAM_NEW to improve the predictions of J over ocean in PBL, although it degrades the J performance over land in PBL compared to MAM_CON/IMN. However, compared with MAM_SIM, J has improved in MAM_NEW by reducing NMBs from −99.6 % to −53.1 %. Compared with MAM_SIM, MAM_NEW increases J at the surface, resulting in an increase in PM_{num} at the surface. The increased J values are due to the lower limit of mass accommodation coefficient of H_2SO_4, resulting in more available H_2SO_4 vapor participating in nucleation. Due to the improved J predictions, aerosol mass and number concentrations increase significantly and the performance of $PM_{2.5}$ and PM_{10} is improved. With all the modified and new treatments, PM_{num} increases, leading to increased AOD by 0.005, CCN at a supersaturation of 0.5 % by 2.7×10^7 cm^{-2}, CDNC by 21.3 cm^{-3}, COT by 0.8, CWP by 3.5 $g\,m^{-2}$, and PWV by 0.012 cm on global average. Due to the aerosol direct and indirect effects, the difference in simulated SWD varies from −33.0 to 34.2 $W\,m^{-2}$ and decreases by 3.4 $W\,m^{-2}$ (∼ 2 %) on a global average. The difference in LWD varies from −30.0 to 16.3 $W\,m^{-2}$ and increases by 0.4 $W\,m^{-2}$

ACPD
13, 27717–27777, 2013

(~ 0.1 %) on a global average (Figure not shown). The difference in SWCF varies from −26.0 to 25.8 W m^{-2} and decreases by 2.8 W m^{-2} (~ 7.5 %) on a global average. The change of radiation can affect meteorological variables. The difference of PBLH varies from −237 to 324 m with a global mean of 0.4 m. The increase of PBLH can increase the vertical mixing in the PBL and decrease the concentration of chemical species at the surface. Precip decreases by 0.1 mm day^{-1}, which can reduce the wet deposition of gaseous and aerosol species.

Compared to MAM_CB05_GE, the simulations with modified or new aerosol treatments (MAM_CON, MAM_CON/IMN, MAM_CON/ISO, MAM_NEW) slightly degrade the predictions of T2, Q2, and LWD (increasing NMBs from −11.1 % up to −16.3 %, from −4.2 % up to −8.3 %, from −0.9 % to −1.4 %, respectively), but improve the predictions of Precip, OLR, CF, COT, and CWP slightly (with 0.6–10.4 % decreases in their NMBs) and CDNC significantly (reducing NMBs from −57.5 % up to −13.4 %). Although the CCN predictions are somewhat degraded in MAM_CON and MAM_CON/IMN, they are improved significantly in MAM_CON/ISO and MAM_NEW (reducing NMBs from −61.6 % to 1.8–6.3 %). Among all new and modified model treatments, the new gas-phase chemistry simulates more gaseous species and improves the predictions of NH_3 over Europe, $PM_{2.5}$ over CONUS and PM_{10} over East Asia. The modified condensation and aqueous-phase chemistry simulate more aerosol species (NO_3^- and Cl^-) and improve the prediction of HNO_3. MAM_CON also improves J in the PBL due to more available H_2SO_4 involving in the homogeneous nucleation using an accommodation coefficient of 0.02 for H_2SO_4 condensation, and improves the predictions of CDNC and AOD significantly. MAM_CON/IMN increases PM_{num} above PBL and $PM_{2.5}$ and PM_{10} over Europe and improves the prediction of $PM_{2.5}$ over CONUS and Europe. MAM_CON/ISO improves the predictions of HNO_3, NH_4^+, $PM_{2.5}$, NO_3^-, and Cl^- over CONUS, NO_3^- and Cl^- over Europe, and CCN over globe, and improves the predictions of SWCF most (with an NMB of 1.6 %).

Large biases in some variables remain in MAM_NEW due to uncertainties in model inputs (e.g., meteorology and emissions) and model treatments (e.g., multi-phase

ACPD
13, 27717–27777, 2013

chemistry, dust emission scheme, cloud microphysics, aerosol activation, SOA formation, and dry and wet deposition). The large NMBs of CO and SO_2 over East Asia, SO_2, NH_3, and NO_2 over Europe, SO_2, and BC over CONUS are likely due to the uncertainties of emissions and the interpolation of emissions from a fine-grid scale in the original emission inventories (e.g., county-based emissions over CONUS) to a large-grid scale used in this work, which can result in large NMBs in secondary aerosols (e.g., SO_4^{2-}, NH_4^+, NO_3^-, thus $PM_{2.5}$ and PM_{10}). Heterogeneous reactions are not included in this work, which may help explain to some extent less oxidation and underpredictions for PM species predictions (e.g., sulfate and nitrate) and overpredictions for gaseous species. The large NMB of O_3 predictions over Europe in MAM_NEW (with an NMB of 62.7 %) is mainly due to a lack of NO_x titration (as indicated by large underpredictions in NO_2) and more production of O_3 from the photolytic reaction of NO_2 resulted from overpredictions of SWD particularly in autumn and winter. Table 5 shows the seasonal statistics for O_3, NO_2, and HNO_3 over Europe in MAM_NEW. During autumn and winter, O_3 is overpredicted by about 100 %~140 %, whereas NO_2 is underpredicted by about −85 %~ −20 %, indicating insufficient NO_x for titration of O_3. SWD is overpredicted by 45.0 $W\,m^{-2}$ (or by 58.4 %), favoring the photolytic reactions of NO_2 to produce O_3. Due to the uncertainties in the NO_x emissions, NO_2 is underpredicted, causing less NO_2 to be oxidized to produce HNO_3, which results in an underprediction of HNO_3 in winter. In autumn, SWD is overpredicted by 42.8 $W\,m^{-2}$ (or by 37.9 %). However, in autumn, although NO_2 is underpredicted due to the uncertainties in the NO_x emissions, HNO_3 mixing ratios are overpredicted. SWD is stronger in autumn than in winter, and mixing ratios of OH are higher due to photolytic reactions of overpredicted O_3 and additional photolytic reactions of VOCs. Therefore, OH can oxidize NO_2 to produce HNO_3, resulting in the overprediction of HNO_3. Simple aqueous-phase chemistry is included in this work, which could result in high uncertainty in predicting aerosols in clouds. Dust emissions are very sensitive to wind speeds. Over Asia, although wind speed decreases less than 0.1 $m\,s^{-1}$ (< 2 %), the concentration of dust decreases by 10 ~ 1000 $\mu g\,m^{-3}$ (or by 10 ~ 50 %), indicating extremely high sensitivity

ACPD
13, 27717–27777, 2013

of dust emissions to wind speed in the dust emission scheme in CAM5.1. Decreased aerosol number concentrations can result in a decrease of CCN and AOD directly. The underpredictions of CDNC are likely due to uncertainties in the model treatments for aerosol activation and cloud microphysics, which then result in large NMBs in COT and CWP. The large biases in OC and TC indicate the uncertainties in the emissions of BC and primary OC, and the treatments for SOA formation. The large NMB in J is likely due to uncertainties in model inputs (e.g., SO_2 emissions) and model treatments (e.g., the accommodation coefficient of H_2SO_4 and missing participants in the current nucleation schemes).

5.6 Impacts of adjusted emissions

The evaluation and analyses of MAM_NEW indicate that some large biases are caused by inaccuracies in the emissions of CO, SO_2, BC, OC, and NH_3. The sensitivity simulation with adjusted emissions of CO, SO_2, BC, OC, and NH_3 (MAM_NEW/EMIS) is performed to further look into such impacts. As shown in Table 4, compared with MAM_NEW, MAM_NEW/EMIS shows an improved performance in the predictions of SO_2, HNO_3, SO_4^{2-}, NH_3, and NH_4^+ over Europe, SO_2, HNO_3, BC, OC, TC, NO_3^-, and Cl^- over CONUS, CO and SO_2 over Asia, and column CO over globe. However, it degrades to some extent the performance of SO_4^{2-} and NH_4^+ over CONUS, $PM_{2.5}$ and PM_{10} over Europe, PM_{10} over Asia, and J over globe. Decreased SO_2 emissions over CONUS result in a decrease of H_2SO_4 and therefore a decrease of SO_4^{2-}. Based on aerosol thermodynamic treatments, decreased SO_4^{2-} will result in decreased NH_4^+. $PM_{2.5}$ and PM_{10} concentrations decrease with adjusted emissions, which is mainly caused by the decrease of dust concentrations in responses to the changes in wind speeds. Adjusted emissions can affect secondary aerosol formations and therefore meteorological and radiative variables can be affected due to the direct and indirect effects of aerosols. As shown in Table 3, compared with MAM_NEW, MAM_NEW/EMIS reduces MB of T2 by 12.7 %, Q2 by 3.6 %, WS10 by 4.8 %, LWD by 9.3 %, SWD by 37.5 %, and CF by

ACPD
13, 27717–27777, 2013

18.9 %, leading to 0.1–1.6 % absolute reduction in their NMBs. This illustrates the sensitivity of meteorology and radiation to the perturbations in emissions through chemistry feedbacks to the climate system.

6 Conclusions and future work

In this work, a new gas-phase chemistry mechanism and several advanced inorganic aerosol treatments have been incorporated into CESM/CAM5.1-MAM7. These include (1) the CB05_GE gas-phase chemical mechanism coupled with MAM7; (2) the condensation and aqueous-phase chemistry involving HNO_3/NO_3^- and HCl/Cl^-; (3) an ion-mediated nucleation parameterization for the new particle formation from ions, (4) an inorganic thermodynamic module, ISORROPIA II, that explicitly simulates thermodynamics of SO_4^{2-}, NH_4^+, NO_3^-, Cl^-, and Na^+ as well as the impact of crustal species, such as Ca^{2+}, K^+, and Mg^{2+}, on aerosol thermodynamics. CB05_GE with new and modified inorganic aerosol treatments in MAM7 simulates 139 species with 273 chemical reactions, which is more accurate than simple gas chemistry coupled with default MAM7. Comparing to the simple gas-phase chemistry, CB05_GE can predict many more gaseous species, and give improved performance for predictions of organic carbon and $PM_{2.5}$ over CONUS, NH_3 and SO_4^{2-} over Europe, SO_2 and PM_{10} over East Asia, and cloud properties such as CF, CDNC, and SWCF. MAM_CON simulates NO_3^- and Cl^-, which are important inorganic aerosols. With species-dependent accommodation coefficients for gas condensation, more H_2SO_4 can participate in homogeneous nucleation, resulting in the improvement of predictions of $PM_{2.5}$, PM_{10}, J, CDNC, and SWCF. IMN can increase the predictions of J and PM_{num} in the upper atmosphere and thus improve the predictions of AOD, CCN, and cloud properties, and SWCF over globe, $PM_{2.5}$ over CONUS and Europe, PM_{10} over Europe and East Asia, and PM composition over Europe. ISORROPIA II can improve the predictions of major gas and aerosol species significantly, including HNO_3, NH_4^+, NO_3^-, Cl^-, BC, OC, TC, and $PM_{2.5}$

ACPD
13, 27717–27777, 2013

over CONUS, SO_2, NH_3, NO_2, SO_4^{2-}, NH_4^+, NO_3^-, and Cl^- over Europe, and CO and SO_2 over East Asia. Such improvements lead to improved predictions of T2, Q2, Precip, SWD, SWCF, and CCN at a supersaturation of 0.5 % over globe. The new and modified inorganic aerosol treatments appreciably improve the predictions of Precip, OLR, CF, COT, CWP, PWV, CCN, CDNC, SWCF, *J* over globe, and HNO_3, NH_4^+ (CONUS), $PM_{2.5}$, and PM_{10}. The sensitivity simulation with adjusted emissions further improves model predictions of CO and SO_2 over East Asia, SO_2, HNO_3, NO_3^-, Cl^-, BC, OC, and TC over CONUS, SO_2, NH_3, NH_4^+, HNO_3., NO_3^-, and Cl^- over Europe, and column CO, T2, Q2, WS10, and SWD over globe. The change of emissions can affect primary gaseous precursors directly, and secondary gaseous species indirectly through gas-phase chemistry. Meanwhile, secondary aerosols can be affected by gaseous precursors, and therefore have impacts on cloud properties as well as direct and indirect effects on radiation and meteorology. Reducing the uncertainty of emissions can thus help reduce the model biases significantly.

Additional uncertainties exist in the model treatments. For example, the large biases in the predictions of O_3 over Europe are mainly due to insufficient NO_x titration resulting from the uncertainties in the NO_x emissions, which also results in large biases in the predictions of NO_2 and HNO_3 over Europe. The large biases in PM_{10} over East Asia and Europe may be mainly due to the inaccurate predictions of dust, which is very sensitive to simulated wind speeds. In the default and modified nucleation treatments, it only considers H_2SO_4, NH_3, H_2O, and ions involving in the new particle formation. Missing species (e.g., organics, iodine compounds, and DMS) may also contribute to the new particle formation. Uncertainties in treating organic gas-aerosol partitioning may contribute to the inaccurate predictions of SOA, OC, TC, and PM. The large biases in CDNC, COT, and LWP indicate the uncertainties in cloud microphysics schemes and aerosol-cloud interaction parameterizations, which also limit the ability of climate and Earth system models to quantify aerosol indirect effects (Stephens, 2005; Lohmann et al., 2007; Gettelman et al., 2008). The representations of some of those uncertain processes in CESM/CAM5.1 are being further improved. Decadal simulations using im-

ACPD
13, 27717–27777, 2013

proved CESM/CAM5.1 will be conducted in the future to study the interactions among atmospheric chemistry, aerosol, and climate change and reduce associated uncertainties.

Acknowledgements. This work is sponsored by the US NSF EaSM program AGS-1049200. The authors would like to thank Fangqun Yu for providing the IMN scheme, Athanasios Nenes for providing ISORROPIA II, Xiaohong Liu for providing a version of MAM7 that works in CAM5.0 and CAM5.1, Ralf Bennartz for providing CDNC data, Steve J. Ghan and Richard C. Easter for insightful discussions, and Shuai Zhu, a former postdoc researcher of the air quality forecasting laboratory at NCSU for early work on the incorporation of CB05_GE and its coupling with MAM3. MODIS data and CERES data are provided by NASA via http://ladsweb.nascom.nasa.gov and http://ceres.larc.nasa.gov/order_data.php, respectively. Other surface network data were downloaded from their respective web sites. We would like to acknowledge high-performance computing support from Yellowstone (ark:/85065/d7wd3xhc) provided by NCAR's Computational and Information Systems Laboratory, sponsored by the US National Science Foundation.

References

Abdul-Razzak, H. and Ghan, S. J.: A parameterization of aerosol activation – Part 2: Multiple aerosol types, J. Geophys. Res., 105, 6837–6844, 2000.

Adams, P. J. and Seinfeld, J. H.: Predicting global aerosol size distributions in general circulation models, J. Geophys. Res., 107, 4370, doi:10.1029/2001JD001010, 2002.

Appel, K. W., Pouliot, G. A., Simon, H., Sarwar, G., Pye, H. O. T., Napelenok, S. L., Akhtar, F., and Roselle, S. J.: Evaluation of dust and trace metal estimates from the Community Multiscale Air Quality (CMAQ) model version 5.0, Geosci. Model Dev., 6, 883–899, doi:10.5194/gmd-6-883-2013, 2013.

Arstila, H., Korhonen, P., and Kulmala, M.: Ternary nucleation: kinetics and application to water-ammonia-hydrochloric acid system, J. Aerosol Sci., 30, 131–138, doi:10.1016/S0021-8502(98)00033-0, 1999.

Barth, M. C., Rasch, P. J., Kiehl, J. T., Benkovitz, C. M., and Schwartz, S. E.: Sulfur chemistry in the National Center for Atmospheric Research Community Climate Model: description,

ACPD
13, 27717–27777, 2013

evaluation, features and sensitivity to aqueous chemistry, J. Geophys. Res., 105, 1387–1415, 2000.
Berndt, T., Sipilä, M., Stratmann, F., Petäjä, T., Vanhanen, J., Mikkilä, J., Patokoski, J., Taipale, R., Lee Mauldin III, R., and Kulmala, M.: Enhancement of atmospheric H_2SO_4/H_2O nucleation: organic oxidation products versus amines, Atmos. Chem. Phys. Discuss., 13, 16301–16335, doi:10.5194/acpd-13-16301-2013, 2013.
Bennartz, R.: Global assessment of marine boundary layer cloud droplet number concentration from satellite, J. Geophys. Res., 112, D02201, doi:10.1029/2006JD007547, 2007.
Bey, I., Jacob, D. J., Yantosca, R. M., Logan, J. A., Field, B. D., Fiore, A. M., Li, Q., Lui, H. Y., Mickley, L. J., and Schultz, M. G.: Global modeling of tropospheric chemistry with assimilated meteorology: model description and evaluation, J. Geophys. Res., 106, 23073–23095, 2001.
Bretherton, C. S. and Park, S.: A new moist turbulence parameterization in the community atmosphere model, J. Climate, 22, 3422–3448, 2009.
Burkholder, J. B., Curtius, J., Ravishankara, A. R., and Lovejoy, E. R.: Laboratory studies of the homogeneous nucleation of iodine oxides, Atmos. Chem. Phys., 4, 19–34, doi:10.5194/acp-4-19-2004, 2004.
Byun, D. W. and Schere, K. L.: Review of the governing equations, computational algorithms, and other components of the Models-3 Community Multiscale Air Quality (CMAQ) Modeling System, Appl. Mech. Rev., 59, 51–77, 2006.
Cappa, C. D., Lovejoy, E. R., and Ravishankara, A. R.: Evidence for liquid-like and nonideal behavior of a mixture of organic aerosol components, P. Natl. Acad. Sci. USA, 105, 18687–18691, doi:10.1073/pnas.0802144105, 2008.
Collins, W. D., Bitz, C. M., Blackmon, M. L., Bonan, G. B., Bretherton, C. S., Carton, J. A., Chang, P., Doney, S. C., Hack, J. J., Henderson, T. B., Kiehl, J. T., Large, W. G., McKenna, D. S., Santer, B. D., and Smith, R. D.: The Community Climate System Model version3 (CCSM3), J. Climate, 19, 2122–2143, doi:10.1175/JCLI3761.1, 2006.
Dunne, J. P., John, J. G., Adcroft, A. J., Griffies, S. M., Hallberg, R. W., Shevliakova, E., Stouffer, R. J., Cooke, W., Dunne, K. A., Harrison, M. J., Krasting, J. P., Malyshev, S. L., Milly, P. C. D., Phillipps, P. J., Sentman, L. T., Samuels, B. L., Spelman, M. J., Winton, M., Wittenberg, A. T., and Zadeh, N.: GFDL's ESM2 global coupled climate–carbon earth system models – Part 1: Physical formulation and baseline simulation characteristics, J. Climate, 25, 6646–6665, 2012.

ACPD
13, 27717–27777, 2013

Dunne, J. P., John, J. G., Shevliakova, E., Stouffer, R. J., Krasting, J. P., Malyshev, S. L., Milly, P. C. D., Sentman, L. T., Adcroft, A. J., Cooke, W., Dunne, K. A., Griffies, S. M., Hallberg, R. W., Harrison, M. J., Levy, H., Wittenberg, A. T., Phillips, P. J., and Zadeh, N.: GFDL's ESM2 global coupled climate–carbon earth system models – Part 2: Carbon system formulation and baseline simulation characteristics, J. Climate, 26, 2247–2267, 2013.

Dutkiewicz, S., Sokolov, A. P., Scott, J., and Stone, P. H.: A three-dimensional ocean–seaice–carbon cycle model and its coupling to a two-dimensional atmospheric model: uses in climate change studies, MIT JPSPGC Report 122, May, 47 pp., 2005.

Emmons, L. K., Walters, S., Hess, P. G., Lamarque, J.-F., Pfister, G. G., Fillmore, D., Granier, C., Guenther, A., Kinnison, D., Laepple, T., Orlando, J., Tie, X., Tyndall, G., Wiedinmyer, C., Baughcum, S. L., and Kloster, S.: Description and evaluation of the Model for Ozone and Related chemical Tracers, version 4 (MOZART-4), Geosci. Model Dev., 3, 43–67, doi:10.5194/gmd-3-43-2010, 2010.

ENVIRON: Comprehensive Air Quality Model with extensions User's Guide, 5.3 edn., Novato, California, USA, 2010.

Faraji, M., Kimura, Y., McDonald-Buller, E., and Allen, D.: Comparison of the carbon bond and SAPRC photochemical mechanisms under conditions relevant to southeast Texas, Atmos. Environ., 42, 5821–5836, doi:10.1016/j.atmosenv.2007.07.048, 2008.

Fast, J. D., Gustafson Jr., W. I., Easter, R. C., Zaveri, R. A., Barnard, J. C., Chapman, E. G., Grell, G. A., and Peckham, S. E.: Evolution of ozone, particulates, and aerosol direct radiative forcing in the vicinity of Houston using a fully coupled meteorology–chemistry–aerosol model, J. Geophys. Res., 111, D21305, doi:10.1029/2005JD006721, 2006.

Fountoukis, C. and Nenes, A.: ISORROPIA II: a computationally efficient thermodynamic equilibrium model for $K^+-Ca^{2+}-Mg^{2+}-NH4^+-Na^+-SO_4^{2-}-NO_3^--Cl^--H_2O$ aerosols, Atmos. Chem. Phys., 7, 4639–4659, doi:10.5194/acp-7-4639-2007, 2007.

Gent, P. R., Yeager, S. G., Neale, R. B., Levis, S., and Bailey, D. A.: Improvements in a half degree atmosphere/land version of the CCSM, Clim. Dynam., 34, 819–833, doi:10.1007/s00382-009-0614-8, 2010.

Gettelman, A., Morrison, H., and Ghan, S. J.: A new two-moment bulk stratiform cloud microphysics scheme in the community atmosphere model, version 3 (CAM3) – Part 2: Single-column and global results, J. Climate, 21, 3660–3679, 2008.

ACPD
13, 27717–27777, 2013

Ghan, S. J., Liu, X., Easter, R. C., Zaveri, R., Rasch, P. J., and Yoon, J.-H.: Toward a minimal representation of aerosols in climate models: comparative decomposition of aerosol direct, semidirect, and indirect radiative forcing, J. Climate, 25, 6461–6476, 2012.

Guenther, A., Karl, T., Harley, P., Wiedinmyer, C., Palmer, P. I., and Geron, C.: Estimates of global terrestrial isoprene emissions using MEGAN (Model of Emissions of Gases and Aerosols from Nature), Atmos. Chem. Phys., 6, 3181–3210, doi:10.5194/acp-6-3181-2006, 2006.

Heintzenberg, J.: Fine particles in the global troposphere: a review, Tellus B, 41, 149–160, 1989.

Hoffmann, T., O'Dowd, C. D., and Seinfeld, J. H.: Iodine oxide homogeneous nucleation: an explanation for coastal new particle production, Geophys. Res. Lett., 28, 1949–1952, 2001.

Iacono, M. J., Delamere, J. S., Mlawer, E. J., and Clough, S. A.: Evaluation of upper tropospheric water vapor in the NCAR Community Climate Model (CCM3) using modeled and observed HIRS radiances, J. Geophys. Res., 108, 4037, doi:10.1029/2002jd002539, 2003.

Iacono, M. J., Delamere, J. S., Mlawer, E. J., Shephard, M. W., Clough, S. A., and Collins, W. D.: Radiative forcing by long-lived greenhouse gases: calculations with the AER radiative transfer models, J. Geophys. Res., 113, D13103, doi:10.1029/2008jd009944, 2008.

Jacobson, M. Z.: Studying the effect of calcium and magnesium on size-distributed nitrate and ammonium with EQUISOLV II, Atmos. Environ., 33, 3635–3649, 1999.

Jacobson, M. Z.: Short-term effects of controlling fossil-fuel soot, biofuel soot and gases, and methane on climate, arctic ice, and air pollution health, J. Geophys. Res., 115, D14209, doi:10.1029/2009JD013795, 2010.

Karamchandani, P., Zhang, Y., Chen, S.-Y., and Balmori-Bronson, R.: Development of an extended chemical mechanism for global-through-urban applications, Atmospheric Pollution Research, 3, 1–24, 2012.

Kim, Y., Sartelet, K., and Seigneur, C.: Formation of secondary aerosols over Europe: comparison of two gas-phase chemical mechanisms, Atmos. Chem. Phys., 11, 583–598, doi:10.5194/acp-11-583-2011, 2011.

Koloutsou-Vakakis, S., Rood, M. J., Nenes, A., and Pilinis, C.: Modeling of aerosol properties related to direct climate forcing, J. Geophys. Res., 103, 17009–17032, doi:10.1029/98JD00068, 1998.

ACPD
13, 27717–27777, 2013

Kuang, C., McMurry, P. H., McCormick, A. V., and Eisele, F. L.: Dependence of nucleation rates on sulfuric acid vapor concentration in diverse atmospheric locations, J. Geophys. Res., 113, D10209, doi:10.1029/2007JD009253, 2008.

Kuang, C., McMurry, P. H., and McCormick, A. V.: Determination of cloud condensation nuclei production from measured new particle formation events, Geophys. Res. Lett., 36, L09822, doi:10.1029/2009GL037584, 2009.

Kulmala, M., Vehkamaki, H., Petaja, T., Dal Maso, M., Lauri, A., Kerminen, V.-M., Birmili, W., and McMurry, P.: Formation and growth rates of ultrafine atmospheric particles: a review of observations, J. Aerosol Sci., 35, 143–176, 2004.

Kulmala, M., Lehtinen, K. E. J., and Laaksonen, A.: Cluster activation theory as an explanation of the linear dependence between formation rate of 3nm particles and sulphuric acid concentration, Atmos. Chem. Phys., 6, 787–793, doi:10.5194/acp-6-787-2006, 2006.

Kurtén, T., Loukonen, V., Vehkamäki, H., and Kulmala, M.: Amines are likely to enhance neutral and ion-induced sulfuric acid-water nucleation in the atmosphere more effectively than ammonia, Atmos. Chem. Phys., 8, 4095–4103, doi:10.5194/acp-8-4095-2008, 2008.

Lamarque, J.-F., Emmons, L. K., Hess, P. G., Kinnison, D. E., Tilmes, S., Vitt, F., Heald, C. L., Holland, E. A., Lauritzen, P. H., Neu, J., Orlando, J. J., Rasch, P. J., and Tyndall, G. K.: CAM-chem: description and evaluation of interactive atmospheric chemistry in the Community Earth System Model, Geosci. Model Dev., 5, 369–411, doi:10.5194/gmd-5-369-2012, 2012.

Lamarque, J.-F., Shindell, D. T., Josse, B., Young, P. J., Cionni, I., Eyring, V., Bergmann, D., Cameron-Smith, P., Collins, W. J., Doherty, R., Dalsoren, S., Faluvegi, G., Folberth, G., Ghan, S. J., Horowitz, L. W., Lee, Y. H., MacKenzie, I. A., Nagashima, T., Naik, V., Plummer, D., Righi, M., Rumbold, S. T., Schulz, M., Skeie, R. B., Stevenson, D. S., Strode, S., Sudo, K., Szopa, S., Voulgarakis, A., and Zeng, G.: The Atmospheric Chemistry and Climate Model Intercomparison Project (ACCMIP): overview and description of models, simulations and climate diagnostics, Geosci. Model Dev., 6, 179–206, doi:10.5194/gmd-6-179-2013, 2013.

Lawrence, D. M., Oleson, K. W., Flanner, M. G., Thornton, P. E., Swenson, S. C., Lawrence, P. J., Zeng, X., Yang, Z.-L., Levis, S., Sakaguchi, K., Bonan, G. B., and Slater, A. G.: Parameterization improvements and functional and structural advances in version 4 of the Community Land Model, J. Adv. Model. Earth Syst., 3, doi:10.1029/2011MS000045, 2011.

ACPD
13, 27717–27777, 2013

Liao, H., Adams, P. J., Chung, S. H., Seinfeld, J. H., Mickley, L. J., and Jacob, D. J.: Interactions between tropospheric chemistry and aerosols in a unified general circulation model, J. Geophys. Res., 108, 4001, doi:10.1029/2001JD001260, 2003.

Liu, X., Easter, R. C., Ghan, S. J., Zaveri, R., Rasch, P., Shi, X., Lamarque, J.-F., Gettelman, A., Morrison, H., Vitt, F., Conley, A., Park, S., Neale, R., Hannay, C., Ekman, A. M. L., Hess, P., Mahowald, N., Collins, W., Iacono, M. J., Bretherton, C. S., Flanner, M. G., and Mitchell, D.: Toward a minimal representation of aerosols in climate models: description and evaluation in the Community Atmosphere Model CAM5, Geosci. Model Dev., 5, 709–739, doi:10.5194/gmd-5-709-2012, 2012.

Lohmann, U., Stier, P., Hoose, C., Ferrachat, S., Kloster, S., Roeckner, E., and Zhang, J.: Cloud microphysics and aerosol indirect effects in the global climate model ECHAM5-HAM, Atmos. Chem. Phys., 7, 3425–3446, doi:10.5194/acp-7-3425-2007, 2007.

Luecken, D. J., Phillips, S., Sarwar, G., and Jang, C.: Effects of using the CB05 vs. SAPRC99 vs. CB4 chemical mechanism on model predictions: ozone and gas-phase photochemical precursor concentrations, Atmos. Environ., 42, 5805–5820, doi:10.1016/j.atmosenv.2007.08.056, 2008.

Marsh, A. R. W. and McElory, W. J.: The dissociation constant and Henry's law constant of HCl in aqueous solution, Atmos. Environ., 19, 1075–1080, 1985.

Martensson, E. M., Nilsson, E. D., deLeeuw, G., Cohen, L. H., and Hansson, H. C.: Laboratory simulations and parameterization of the primary marine aerosol production, J. Geophys. Res., 108, 4297, doi:10.1029/2002JD002263, 2003.

Meng, Z. and Seinfeld, J. H.: Time scales to achieve atmospheric gas-aerosol equilibrium for volatile species, Atmos. Environ., 30, 2889–2900, 1996.

Meng, Z., Dabdub, D., and Seinfeld, J. H.: Size- and chemically-resolved model of atmospheric aerosol dynamics. J. Geophys. Res., 103, 3419–3435, 1998.

Merikanto, J., Napari, I., Vehkamaki, H., Anttila, T., and Kulmala, M.: New parameterization of sulfuric acid-ammonia-water ternary nucleation rates at tropospheric conditions, J. Geophys. Res., 112, D15207, doi:10.1029/2006JD007977, 2007.

Metzger, S. and Lelieveld, J.: Reformulating atmospheric aerosol thermodynamics and hygroscopic growth into fog, haze and clouds, Atmos. Chem. Phys., 7, 3163–3193, doi:10.5194/acp-7-3163-2007, 2007.

Metzger, S., Dentener, F. J., Lelieveld, J., and Pandis, S. N.: Gas/aerosol partitioning I: a computationally efficient model, J. Geophys. Res., 107, 4312, doi:10.1029/2001JD001102, 2002.

ACPD
13, 27717–27777, 2013

Metzger, S., Steil, B., Xu, L., Penner, J. E., and Lelieveld, J.: New representation of water activity based on a single solute specific constant to parameterize the hygroscopic growth of aerosols in atmospheric models, Atmos. Chem. Phys., 12, 5429–5446, doi:10.5194/acp-12-5429-2012, 2012.

Mlawer, E. J., Taubman, S. J., Brown, P. D., Iacono, M. J., and Clough, S. A.: Radiative transfer for inhomogeneous atmospheres: RRTM, a validated correlated-*k* model for the longwave, J. Geophys. Res., 102, 16663–16682, 1997.

Monier, E., Scott, J. R., Sokolov, A. P., Forest, C. E., and Schlosser, C. A.: An integrated assessment modelling framework for uncertainty studies in global and regional climate change: the MIT IGSM-CAM (version 1.0), Geosci. Model Dev. Discuss., 6, 2213–2248, doi:10.5194/gmdd-6-2213-2013, 2013.

Morrison, H. and Gettelman, A.: A new two-moment bulk stratiform cloud microphysics scheme in the community atmosphere model, version 3 (CAM3) – Part 1: Description and numerical tests, J. Climate, 21, 3642–3659, 2008.

Nenes, A., Pandis, S. N., and Pilinis, C.: ISORROPIA: a new thermodynamic equilibrium model for multiphase multicomponent inorganic aerosols, Aquat. Geochem., 4, 123–152, 1998.

O'Dowd, C. D., Jimenez, J. L., Bahreini, R., Flagan, R. C., Seinfeld, J. H., Hämeri, K., Pirjola, L., Kulmala, M., Jennings, S. G., and Hoffmann, T.: Marine aerosol formation from biogenic iodine emissions, Nature, 417, 632–636, doi:10.1038/nature00775, 2002.

Olerud, D. and Sims, A.: MM5 2002 Modeling in Support of VISTAS (Visibility Improvement – State and Tribal Association of the Southeast), Report, Baron Advanced Meteorological Systems, LLC, Raleigh, NC, August, 2004.

Park, S. and Bretherton, C. S.: The university of Washington shallow convection and moist turbulence schemes and their impact on climate simulations with the community atmosphere model, J. Climate, 22, 3449–3469, 2009.

Pechtl, S., Lovejoy, E. R., Burkholder, J. B., and von Glasow, R.: Modeling the possible role of iodine oxides in atmospheric new particle formation, Atmos. Chem. Phys., 6, 505–523, doi:10.5194/acp-6-505-2006, 2006.

Pierce, J. R. and Adams, P. J.: Uncertainty in global CCN concentrations from uncertain aerosol nucleation and primary emission rates, Atmos. Chem. Phys., 9, 1339–1356, doi:10.5194/acp-9-1339-2009, 2009.

Raes, F., Augustin, J., and Vandingenen, R.: The role of ion-induced aerosol formation in the lower atmosphere, J. Aerosol Sci., 17, 466–470, doi:10.1016/0021-8502(86)90135-7, 1986.

ACPD
13, 27717–27777, 2013

Reiter, R.: Phenomena in Atmospheric and Environmental Electricity, Elsevier, New York, 1992.
Roeckner, E., Bauml, G., Bonaventura, L., Brokopf, R., Esch, M., Giorgetta, M., Hagemann, S., Kirchner, I., Kornblueh, L., Manzini, E., Rhodin, A., Schlese, U., Schulzweida, U., and Tompkins, A.: The atmospheric general circulation model ECHAM 5 – PART 1: Model description, MPI Technical Report 349, Max Planck Institute for Meteorology, Hamburg, Germany, 2003.
Roeckner, E., Brokopf, R., Esch, M., Giorgetta, M. A., Hagemann, S., Kornblueh, L., Manzini, E., Schlese, U., and Schulzweida, U.: Sensitivity of simulated climate to horizontal and vertical resolution in the ECHAM5 atmosphere model, J. Climate, 19, 3771–3791, 2006.
Sander, S. P., Friedl, R. R., Golden, D. M., Kurylo, M. J., Huie, R. E., Orkin, V. L., Moortgat, G. K., Ravishankara, A. R., Kolb, C. E., Molina, M. J., and Finlayson-Pitts, B. J.: Chemical kinetics and photochemical data for use in atmospheric studies, National Aeronautics and Space Administration, Jet Propulsion Laboratory California Institute of Technology Pasadena, California, 2003.
Sarwar, G., Luecken, D., Yarwood, G., Whitten, G., and Carter, W. P. L.: Impact of an updated carbon bond mechanism on predictions from the community multiscale air quality model, J. Appl. Meteorol. Clim., 47, 3–14, doi:10.1175/2007JAMC1393.1, 2008.
Schwartz, S. E.: Gas- and aqueous-phase chemistry of HO_2 in liquid water clouds, J. Geophys. Res., 89, 11589–11598, 1984.
Seinfeld, J. H. and Pandis, S. N.: Atmospheric Chemistry and Physics: From Air Pollution to Climate Change, 2 edn., John Wiley & Sons, Inc., 2006.
Shindell, D. T., Lamarque, J.-F., Schulz, M., Flanner, M., Jiao, C., Chin, M., Young, P. J., Lee, Y. H., Rotstayn, L., Mahowald, N., Milly, G., Faluvegi, G., Balkanski, Y., Collins, W. J., Conley, A. J., Dalsoren, S., Easter, R., Ghan, S., Horowitz, L., Liu, X., Myhre, G., Nagashima, T., Naik, V., Rumbold, S. T., Skeie, R., Sudo, K., Szopa, S., Takemura, T., Voulgarakis, A., Yoon, J.-H., and Lo, F.: Radiative forcing in the ACCMIP historical and future climate simulations, Atmos. Chem. Phys., 13, 2939–2974, doi:10.5194/acp-13-2939-2013, 2013.
Sihto, S.-L., Kulmala, M., Kerminen, V.-M., Dal Maso, M., Petäjä, T., Riipinen, I., Korhonen, H., Arnold, F., Janson, R., Boy, M., Laaksonen, A., and Lehtinen, K. E. J.: Atmospheric sulphuric acid and aerosol formation: implications from atmospheric measurements for nucleation and early growth mechanisms, Atmos. Chem. Phys., 6, 4079–4091, doi:10.5194/acp-6-4079-2006, 2006.

ACPD
13, 27717–27777, 2013

Sokolov, A. P., Schlosser, C. A., Dutkiewicz, S., Paltsev, S., Kicklighter, D., Jacoby, H. D., Prinn, R. G., Forest, C. E., Reilly, J. M., Wang, C., Felzer, B., Sarofim, M. C., Scott, J., Stone, P. H., Melillo, J. M., and Cohen, J.: The MIT Integrated Global System Model (IGSM) Version 2: model description and baseline evaluation, MIT JPSPGC Report 124, July, 40 pp., 2005.

Spracklen, D. V., Carslaw, K. S., Kulmala, M., Kerminen, V.-M., Mann, G. W., and Sihto, S.-L.: The contribution of boundary layer nucleation events to total particle concentrations on regional and global scales, Atmos. Chem. Phys., 6, 5631–5648, doi:10.5194/acp-6-5631-2006, 2006.

Stephens, G. L.: Cloud feedbacks in the climate system: a critical review, J. Climate, 18, 237–273, 2005.

Stier, P., Feichter, J., Kinne, S., Kloster, S., Vignati, E., Wilson, J., Ganzeveld, L., Tegen, I., Werner, M., Balkanski, Y., Schulz, M., Boucher, O., Minikin, A., and Petzold, A.: The aerosol-climate model ECHAM5-HAM, Atmos. Chem. Phys., 5, 1125–1156, doi:10.5194/acp-5-1125-2005, 2005.

Usoskin, I. G. and Kovaltsov, G. A.: Cosmic ray induced ionization in the atmosphere: full modeling and practical applications, J. Geophys. Res., 111, D21206, doi:10.1029/2006JD007150, 2006.

van Dingenen, R. and Raes, F.: Ternary nucleation of methane sulphonic acid, sulphuric acid and water vapour, J. Aerosol Sci., 24, 1–17, doi:10.1016/0021-8502(93)90081-J, 1993.

Van Pelt, R. S. and Zobeck, T. M.: Chemical constituents of fugitive dust, Environ. Monit. Assess., 130, 3–16, doi:10.1007/s10661-006-9446-8, 2007.

Vehkamaki, H., Kulmala, M., Napari, I., Lehtinen, K. E. J., Timmreck., C., Noppel, M., and Laaksonen, A.: An improved parameterization for sulfuric acid-water nucleation rates for tropospheric and stratospheric conditions, J. Geophys. Res.-Atmos., 107, 4622, doi:10.1029/2002JD002184, 2002.

Wang, K., Zhang, Y., Nenes, A., and Fountoukis, C.: Implementation of dust emission and chemistry into the Community Multiscale Air Quality modeling system and initial application to an Asian dust storm episode, Atmos. Chem. Phys., 12, 10209–10237, doi:10.5194/acp-12-10209-2012, 2012.

Wang, M. and Penner, J. E.: Aerosol indirect forcing in a global model with particle nucleation, Atmos. Chem. Phys., 9, 239–260, doi:10.5194/acp-9-239-2009, 2009.

ACPD
13, 27717–27777, 2013

Wexler, A. S. and Seinfeld, J. H.: Second-generation inorganic aerosol model, Atmos. Environ., 25A, 2731–2748, 1991.

Young, P. J., Archibald, A. T., Bowman, K. W., Lamarque, J.-F., Naik, V., Stevenson, D. S., Tilmes, S., Voulgarakis, A., Wild, O., Bergmann, D., Cameron-Smith, P., Cionni, I., Collins, W. J., Dalsøren, S. B., Doherty, R. M., Eyring, V., Faluvegi, G., Horowitz, L. W., Josse, B., Lee, Y. H., MacKenzie, I. A., Nagashima, T., Plummer, D. A., Righi, M., Rumbold, S. T., Skeie, R. B., Shindell, D. T., Strode, S. A., Sudo, K., Szopa, S., and Zeng, G.: Pre-industrial to end 21st century projections of tropospheric ozone from the Atmospheric Chemistry and Climate Model Intercomparison Project (ACCMIP), Atmos. Chem. Phys., 13, 2063–2090, doi:10.5194/acp-13-2063-2013, 2013.

Yu, F.: From molecular clusters to nanoparticles: second-generation ion-mediated nucleation model, Atmos. Chem. Phys., 6, 5193–5211, doi:10.5194/acp-6-5193-2006, 2006.

Yu, F.: Ion-mediated nucleation in the atmosphere: key controlling parameters, implications, and look-up table, J. Geophys. Res., 115, D03206, doi:10.1029/2009JD012630, 2010.

Yu, F. and Luo, G.: Simulation of particle size distribution with a global aerosol model: contribution of nucleation to aerosol and CCN number concentrations, Atmos. Chem. Phys., 9, 7691–7710, doi:10.5194/acp-9-7691-2009, 2009.

Yu, F. and Turco, R. P.: Ultrafine aerosol formation via ion-mediated nucleation, Geophys. Res. Lett., 27, 883–886, doi:10.1029/1999GL011151, 2000.

Yu, F. and Turco, R. P.: From molecular clusters to nanoparticles: the role of ambient ionization in tropospheric aerosol formation, J. Geophys., Res., 106, 4797–4814, doi:10.1029/2000JD900539, 2001.

Yu, F., Wang, Z., Luo, G., and Turco, R.: Ion-mediated nucleation as an important global source of tropospheric aerosols, Atmos. Chem. Phys., 8, 2537–2554, doi:10.5194/acp-8-2537-2008, 2008.

Yu, F., Luo, G., Bates, T. S., Anderson, B., Clarke, A., Kapustin, V., Yantosca, R. M., Wang, Y., and Wu, S.: Spatial distributions of particle number concentrations in the global troposphere: simulations, observations, and implications for nucleation mechanisms, J. Geophys., Res., 115, D17205, doi:10.1029/2009JD013473, 2010.

Yu, F., Luo, G., Liu, X., Easter, R. C., Ma, X., and Ghan, S. J.: Indirect radiative forcing by ion-mediated nucleation of aerosol, Atmos. Chem. Phys., 12, 11451–11463, doi:10.5194/acp-12-11451-2012, 2012.

ACPD
13, 27717–27777, 2013

Zaveri, R. A., Easter, R. C., and Peters, L. K.: A computationally efficient multicomponent equilibrium solver for aerosols (MESA), J. Geophys. Res., 110, D24203, doi:10.1029/2004JD005618, 2005.

Zender, C. S., Bian, H., and Newman, D.: The mineral Dust Entrainment And Deposition (DEAD) model: description and 1990s dust climatology, J. Geophys. Res., 108, 4416, doi:10.1029/2002JD002775, 2003.

Zhang, G. J. and McFarlane, N. A.: Sensitivity of climate simulations to the parameterization of cumulus convection in the Canadian Climate Centre general circulation model, Atmos. Ocean, 33, 407–446, 1995.

Zhang, Y., Bischof, C. H., Easter, R. C., and Wu, P.-T.: Sensitivity analysis of a mixed-phase chemical mechanism using automatic differentiation, J. Geophys. Res., 103, 18953–18979, 1998.

Zhang, Y., Seigneur, C., Seinfeld, J. H., Jacobson, M., Clegg, S. L., Binkowski, F. S.: A comparative review of inorganic aerosol thermodynamic equilibrium modules: similarities, differences, and their likely causes, Atmos. Environ., 34, 117–137, 2000.

Zhang, Y., McMurry, P. H., Yu, F., and Jacobson, M. Z.: A comparative study of nucleation parameterizations: 1. examination and evaluation of the formulations, J. Geophys. Res., 115, D20212, doi:10.1029/2010JD014150, 2010.

Zhang, Y., Chen, Y., Sarwar, G., and Schere, K.: Impacts of gas-phase mechanisms on weather research forecasting model with chemistry (WRF/Chem) predictions: mechanism implementation and comparative evaluation, J. Geophys. Res., 117, D01301, doi:10.1029/2011JD015775, 2012a.

Zhang, Y., Karamchandani, P., Glotfelty, T., Street, D. G., Grell, G., Nenes, A., Yu, F., and Bennartz, R.: Development and initial application of the global-through-urban weather research and forecasting model with chemistry (GU-WRF/Chem), J. Geophys. Res., 117, D20206, doi:10.1029/2012JD017966, 2012b.

Zuend, A., Marcolli, C., Peter, T., and Seinfeld, J. H.: Computation of liquid-liquid equilibria and phase stabilities: implications for RH-dependent gas/particle partitioning of organic-inorganic aerosols, Atmos. Chem. Phys., 10, 7795–7820, doi:10.5194/acp-10-7795-2010, 2010.

ACPD
13, 27717–27777, 2013

Table 1. Simulation design and purposes.

Run Index	Model Configuration	Purpose
MAM_SIM	Simple gas-phase chemistry coupled with default MAM7	A baseline run for the 1st set of simulations (see text)
MAM_CB05_GE	CB05_GE coupled with default MAM7	Differences of MAM_SIM and MAM_CB05_GE indicate the impacts of gas-phase chemical mechanisms
MAM_CON	Same as MAM_CB05_GE, but with explicit treatments for NO_3^-, Cl^-, and Na^+; HNO_3 and HCl condensation and aqueous-phase chemistry; species-dependent accommodation coefficients	A baseline run for the 2nd set of simulations; differences of MAM_SIM and MAM_CB05_GE indicate the impact of modified condensation and aqueous -phase chemistry treatments
MAM_CON/IMN	Same as MAM7_CON, but combine IMN with modified default nucleation parameterizations with a prefactor of 1.0×10^{-8}	Differences of MAM_CON and MAM_CON/IMN indicate the impacts of IMN and the lower prefactor for WP09
MAM_CON/ISO	Same as MAM7_CON, but with ISORROPIA II for aerosol thermodynamics under metastable conditions	Differences between MAM_CON and MAM_IMN/ISO indicate the impacts of explicit aerosol thermodynamics
MAM_NEW	Same as MAM7_CON, but with all modified and new treatments and using a prefactor of 1.0×10^{-9} for default nucleation parameterization	Differences between MAM_CB05_GE and MAM_NEW indicate the impacts of all new and modified treatments for inorganic aerosols
MAM_NEW/EMIS	Same as MAM7_NEW, but with adjusted emissions of SO_2, NH_3, BC, POM, and CO over CONUS, Europe, and East Asia	Differences between MAM_NEW and MAM_NEW/EMIS indicate the impact of emissions

ACPD
13, 27717–27777, 2013

Table 2. Datasets for model evaluation.

Species/Variables	Dataset
Temperature at 2 m (T2)	NCDC
Specific humidity at 2 m (Q2)	NCDC
Wind speed at 10 m (WS10)	NCDC
Precipitation (Precip)	GPCP
Downwelling longwave radiation (LWD)	BSRN
Downwelling shortwave radiation (SWD)	BSRN
Outgoing longwave radiation (OLR)	NOAA/CDC
Cloud fraction (CF)	MODIS
Cloud optical thickness (COT)	MODIS
Cloud water path (CWP)	MODIS
Precipitating water vapor (PWV)	MODIS
Aerosol optical depth (AOD)	MODIS
Column cloud condensation nuclei (CCN) (ocean) at S = 0.5 %	MODIS
Cloud droplet number concentration (CDNC)	BE07
Shortwave cloud radiative forcing (SWCF)	CERES
Carbon monoxide (CO)	Europe: EMEP East Asia: NIES of Japan, TAQMN
Ozone (O_3)	CONUS: CASTNET Europe: Airbase, BDQA, EMEP
Sulfur dioxide (SO_2)	CONUS: CASTNET Europe: Airbase, BDQA, EMEP East Asia: MEP of China, NIES of Japan, TAQMN
Nitric acid (HNO_3)	CONUS: CASTNET Europe: EMEP
Ammonia (NH_3)	Europe: Airbase, EMEP
Nitrogen dioxide (NO_2)	Europe: Airbase, BDQA, EMEP
Sulfate (SO_4^{2-})	CONUS: CASTNET, IMPROVE, STN Europe: Airbase, EMEP
Ammonium (NH_4^+)	CONUS: CASTNET, IMPROVE, STN Europe: Airbase, EMEP
Nitrate (NO_3^-)	CONUS: CASTNET, IMPROVE, STN Europe: Airbase, EMEP
Chloride (Cl^-)	CONUS: IMPROVE Europe: Airbase, EMEP
Organic carbon (OC), Black carbon (BC), Total carbon (TC)	CONUS: IMPROVE, STN
Particulate matter with diameter less than 2.5 µm ($PM_{2.5}$)	CONUS: IMPROVE, STN Europe: BDQA, EMEP
Particulate matter with diameter less than 10 µm (PM_{10})	Europe: Airbase, BDQA, EMEP East Asia: MEP of China, NIES of Japan, TAQMN
Column CO	Globe: MOPITT
Column NO_2	Globe: GOME
Tropospheric ozone residual (TOR)	Globe: TOMS/SBUV
New particle formation rate (J)	Globe: Kulmala et al. (2004); Yu et al. (2008)

NCDC: National Climatic Data Center; GPCP: Global Precipitation Climatology Project; BSRN: Baseline Surface Radiation Network; NOAA/CDC: National Oceanic and Atmospheric Administration Climate Diagnostics Center; MODIS: Moderate Resolution Imaging Spectroradiometer; BE07: Bennartz, 2007; CERES: Clouds and Earth's Radiant Energy System; TOMS/SBUV: the Total Ozone Mapping Spectrometer/the Solar Backscatter UltraViolet; MOPITT: the Measurements Of Pollution In The Troposphere; GOME: Global Ozone Monitoring Experiment; CASTNET: Clean Air Status and Trends Network; IMPROVE: Interagency Monitoring of Protected Visual Environments; STN: Speciation Trends Network; EMEP: European Monitoring and Evaluation Program; BDQA: Base de Données sur la Qualité de l'Air; AirBase: European air quality database; MEP of China: Ministry of Environmental Protection of China; TAQMN: Taiwan Air Quality Monitoring Network; NIES of Japan: National Institute for Environmental Studies of Japan.

ACPD
13, 27717–27777, 2013

Table 3. Mean Bias (MB) and Normalized Mean Bias (NMB, in %) of Meteorological/Radiative Predictions.

Species/Variables	Dataset	Obs.	Simulations MAM_ SIM	MAM_ CB05_GE	MAM_ CON	MAM_ CON/IMN	MAM_ CON/ISO	MAM_ NEW	MAM_ NEW/EMIS
T2 (°C)	NCDC	13.2	−1.4/−10.9[a]	−1.5/−11.1	−2.2/−16.3	−2.0/−15.4	−1.6/−12.4	−1.6/−12.4	−1.4/−10.8
Q2 ($g kg^{-1}$)	NCDC	8.4×10^{-3}	-4.3×10^{-4} /−5.1	-3.5×10^{-4} /−4.2	-6.6×10^{-4} /−7.9	-7.0×10^{-4} /−8.3	-4.6×10^{-4} /−5.5	-4.5×10^{-4} /−5.4	-4.4×10^{-4} /−5.2
WS10 ($m s^{-1}$)[b]	NCDC	3.9	-5.9×10^{-1} /−15.2	-6.1×10^{-1} /−15.6	-6.0×10^{-1} /−15.4	-5.9×10^{-1} /−15.2	-6.1×10^{-1} /−15.6	-6.3×10^{-1} /−16.2	-6.0×10^{-1} /−15.4
Precip ($mm day^{-1}$)	GPCP	2.3	0.3/12.9	0.3/12.9	0.3/12.3	0.2/9.8	0.2/9.7	0.2/10.7	0.3/11.0
LWD ($W m^{-2}$)[c]	BSRN	312.5	−3.4/−1.1	−2.9/−0.9	−4.2/−1.3	−4.5/−1.4	−4.2/−1.3	−3.8/−1.2	−3.5/−1.1
SWD ($W m^{-2}$)[d]	BSRN	181.2	−2.0/−1.1	−4.2/−2.3	−11.8/−6.5	−11.0/−6.1	−3.9/−2.2	−6.8/−3.7	−4.2/−2.3
OLR ($W m^{-2}$)	NOAA-CDC	214.4	8.8/4.1	8.1/3.8	4.9/2.3	4.9/2.3	6.2/2.9	6.9/3.2	6.9/3.2
SWCF ($W m^{-2}$)	CERES	−41.0	3.2/7.9	2.7/6.5	−2.2/−5.3	2.3/−5.6	−0.7/1.6	−0.4/0.9	−0.6/1.4
CF (%)	MODIS	66.9	−1.4/−2.0	−1.0/−1.5	0.5/0.8	0.7/1.0	−0.5/−0.8	−0.4/−0.6	−0.3/−0.5
COT	MODIS	17.1	−10.2/−59.5	−10.1/−58.8	−8.4/−49.2	−8.3/−48.4	−9.4/−55.1	−9.4/−54.9	−9.4/−55.2
CWP ($g m^{-2}$)	MODIS	148.1	−115.1/−77.7	−114.7/−77.4	−105.8/−71.4	−105.4/−71.2	−111.7/−75.4	−111.7/−75.4	−111.9/−75.5
PWV (cm)	MODIS	1.9	-2.5×10^{-2} /−1.3	-1.8×10^{-2} /−0.9	-3.3×10^{-2} /−1.7	-3.9×10^{-2} /−2.0	-1.8×10^{-2} /−0.9	-1.4×10^{-2} /−0.7	-1.2×10^{-2} /−0.6
AOD	MODIS	1.5×10^{-1}	-5.5×10^{-2} /−36.1	-5.2×10^{-2} /−33.9	-3.0×10^{-2} /−19.8	-2.6×10^{-2} /−17.1	-5.3×10^{-2} /−34.4	-5.0×10^{-2} /−32.9	-5.2×10^{-2} /−34.0
Column CCN (ocean) at $S = 0.5\%$ (cm^{-2})	MODIS	2.4×10^{8}	-1.9×10^{8} /−76.4	-1.9×10^{8} /−78.6	-6.7×10^{7} /−27.5	-4.6×10^{7} /−18.8	-1.5×10^{8} /−62.7	-1.6×10^{8} /−65.3	-1.6×10^{8} /−66.6
CDNC (cm^{-3})	BE07	113.1	−67.7 /−59.9	−66.5/−58.8	−23.4/−20.7	−20.0/−17.7	−48.1/−42.5	−46.4/−41.0	−46.1/−40.8

[a] The values of MBs and NMBs are expressed as MB/NMB.
[b] The lower limit value for observed WS10 is 1.54 $m s^{-1}$ based on Olerud and Sims (2004).
[c] The lower and upper values for observed LWD are 50 and 700 $W m^{-2}$, respectively (http://www.pangaea.de).
[d] The lower and upper values for observed SWD are −10 and 3000 $W m^{-2}$, respectively (http://www.pangaea.de).

ACPD
13, 27717–27777, 2013

Table 4. Mean Bias (MB) and Normalized Mean Bias (NMB, in %) of Chemical Predictions.

Species/ variables	Domain	Obs.	Simulations MAM_SIM	MAM_CB05_GE	MAM_CON	MAM_CON/ IMN	MAM_CON/ ISO	MAM_NEW	MAM_NEW/ EMIS
CO	Europe	123.0	–	−10.6/−8.6	−8.0/−6.5	−15.1/−12.3	−9.0/−7.3	−4.2/−3.4	14.9/12.1
	East Asia	0.6	–	−0.5/−82.1	−0.5/−82.0	−0.5/−81.8	−0.5/−81.8	−0.5/−82.0	−0.5/−78.7
SO_2	CONUS	3.9	10.3/264.8*	10.5/270.1	11.7/301.2	11.2/286.1	11.5/295.8	11.4/291.8	5.9/152.2
	Europe	6.8	6.6/97.5	7.0/103.2	8.4/123.0	6.8/100.3	7.8/114.7	8.9/130.7	0.0/0.3
	East Asia	12.5	−7.9/−63.0	−7.7/−61.3	−7.7/−61.4	−7.7/−61.8	−7.6/−61.0	−7.7/−61.2	−6.7/−53.4
NH_3	Europe	9.4	−7.7/−82.0	−7.6/−80.8	−8.2/−86.8	−8.3/−87.8	−8.0/−84.7	−7.9/−84.3	−7.3/−77.5
NO_2	Europe	20.2	–	−15.6/−77.0	−15.0/−74.1	−15.5/−76.5	−15.2/−75.2	−15.0/−74.1	−15.3/−75.9
O_3	CONUS	34.6	–	10.0/28.9	8.0/23.0	7.9/22.7	9.8/28.4	9.5/27.4	9.8/28.1
	Europe	53.5	–	36.7/68.6	30.9/57.7	31.0/58.0	34.1/63.7	33.5/62.7	34.9/65.2
HNO_3	CONUS	1.5	–	1.0/68.1	−0.9/−60.2	−0.9/−59.7	0.2/15.8	0.3/17.7	0.1/4.1
	Europe	0.5	–	1.3/268.5	−0.2/−34.1	−0.2/−35.8	0.4/86.1	0.4/83.6	0.4/73.8
SO_4^{2-}	CONUS	2.6	−0.1/−5.1	−0.2/−7.2	4.4×10^{-2}/1.7	4.2×10^{-2}/1.6	−0.2/−7.9	−0.2/−6.3	−0.7/−28.4
	Europe	2.2	0.8/36.5	0.7/33.1	0.9/40.3	0.8/35.8	0.7/32.6	0.9/39.4	−0.2/−7.2
NH_4^+	CONUS	1.4	−0.4/−32.1	−0.6/−39.6	0.3/20.0	0.3/19.7	−0.1/−6.4	−0.1/−6.5	−0.2/−13.1
	Europe	1.2	−0.1/−9.1	−0.2/18.3	1.0/85.0	0.8/65.7	0.6/49.4	0.7/54.8	0.4/32.5
NO_3^-	CONUS	1.0	–	–	2.0/198.2	1.9/192.7	$-4.8 \times 10^{-2}/-4.8$	−0.1/−9.6	4.0×10^{-3}/0.4
	Europe	2.0	–	–	1.4/67.8	1.0/49.4	−0.1/−4.3	$-4.0 \times 10^{-2}/-2.0$	0.1/5.2
Cl^-	CONUS	0.1	–	–	0.4/359.9	0.4/373.1	$-1.5 \times 10^{-2}/-14.5$	$-1.8 \times 10^{-2}/-17.5$	$-2.8 \times 10^{-3}/-2.8$
	Europe	0.7	–	–	0.7/102.8	0.6/89.9	2.1×10^{-3}/0.3	1.4×10^{-2}/2.0	$-4.7 \times 10^{-2}/-6.7$
BC	CONUS	0.6	−0.3/−54.6	−0.3/−55.8	−0.3/−54.7	−0.3/−54.6	−0.3/−53.8	−0.3/−54.3	−0.2/−29.4
OC	CONUS	2.0	−0.9/−46.0	−0.8/−39.5	−0.8/−38.6	−0.8/−39.0	−0.7/−37.2	−0.7/−37.3	−0.7/−36.6
TC	CONUS	2.5	−1.2/−47.9	−1.1/−43.1	−1.1/−42.2	−1.1/−42.5	−1.0/−40.9	−1.0/−41.1	−0.9/−35.0
$PM_{2.5}$	CONUS	7.9	−3.0/−37.6	−2.9/−36.8	1.6/20.1	1.3/16.7	−0.1/−1.7	−1.0/−13.2	−1.1/−13.5
	Europe	14.5	−6.1/−41.8	−6.6/−45.3	−0.8/−5.5	−0.1/−0.9	−3.5/−24.4	−2.6/−17.7	−3.9/−27.2
PM_{10}	Europe	25.7	−8.2/−31.8	−9.2/−35.8	−3.2/−12.3	−2.7/−10.5	−4.8/−18.5	−4.3/−16.6	−4.8/−18.8
	East Asia	118.5	−80.0/−67.5	−73.6/−62.1	−62.6/−52.8	−57.7/−48.7	−70.0/−59.1	−53.0/−44.7	−70.3/−59.3
Col.CO	Globe	1.3×10^{18}	– –	$-7.4 \times 10^{16}/-5.7$	$-5.7 \times 10^{16}/-4.4$	$-6.3 \times 10^{16}/-4.8$	$-6.4 \times 10^{16}/-4.9$	$-6.3 \times 10^{16}/-4.8$	2.3×10^{16}/1.8
Col.NO_2	Globe	4.7×10^{14}	–	1.9×10^{14}/40.5	1.4×10^{14}/30.4	1.4×10^{14}/30.0	1.8×10^{14}/37.5	1.8×10^{14}/37.2	1.8×10^{14}/37.3
TOR	Globe	30.3	–	−1.1/−3.7	−2.7/−9.0	−2.9/−9.6	−1.5/−4.9	−1.6/−5.2	−1.5/−4.9
J	Globe	0.6	−0.6/−99.6	−0.5/−99.5	−0.1/−12.8	−0.3/−49.6	0.2/36.1	−0.3/−53.1	−0.3/−62.0

The units are CO, ppb (over Europe) and ppm (over East Asia); SO_2, ppb (over East Asia) and $\mu g\,m^{-3}$ (over CONUS and Europe); O_3, ppb (over CONUS) and $\mu g\,m^{-3}$ (over Europe); column CO and NO_2, molecules cm^{-2}; TOR, DU; J, $cm^{-3}\,s^{-1}$. All other concentrations are in $\mu g\,m^{-3}$.
*The values of MBs and NMBs are expressed as MB/NMB.

ACPD
13, 27717–27777, 2013

Table 5. The observed values and the mean bias (MB) and normalized mean bias (NMB, in %) of predictions of O_3 NO_2, and HNO_3 mixing ratios over Europe in MAM_NEW.

	Network		Obs ($\mu g\,m^{-3}$)	MAM_NEW
Winter	Airbase	O_3	37.7	37.5/99.6*
		NO_2	26.0	−18.4/−70.9
	BDQA	O_3	31.0	43.2/139.2
		NO_2	30.6	−25.0/−81.9
	EMEP	O_3	50.7	25.0/49.3
		NO_2	9.0	−0.7/−7.8
		HNO_3	0.5	-4.9×10^{-3}/1.0
Spring	Airbase	O_3	63.1	37.7/59.7
		NO_2	20.0	−15.4/−77.1
	BDQA	O_3	59.6	39.3/65.9
		NO_2	23.6	−20.5/−87.0
	EMEP	O_3	75.0	26.9/35.9
		NO_2	5.9	−1.0/−17.2
		HNO_3	0.4	0.5/144.5
Summer	Airbase	O_3	64.9	28.6/44.0
		NO_2	16.2	−11.8/−72.8
	BDQA	O_3	64.5	30.0/46.5
		NO_2	18.7	−15.1/−80.9
	EMEP	O_3	72.2	19.0/26.3
		NO_2	4.7	−0.3/−6.2
		HNO_3	0.5	0.8/169.6
Autumn	Airbase	O_3	40.5	39.0/96.4
		NO_2	21.7	−16.4/−75.6
	BDQA	O_3	35.7	45.2/126.5
		NO_2	24.8	−21.1/−85.2
	EMEP	O_3	51.7	26.5/51.2
		NO_2	6.6	−1.4/−21.1
		HNO_3	0.6	0.3/45.0

*The values of MBs and NMBs are expressed as MB/NMB.

ACPD
13, 27717–27777, 2013

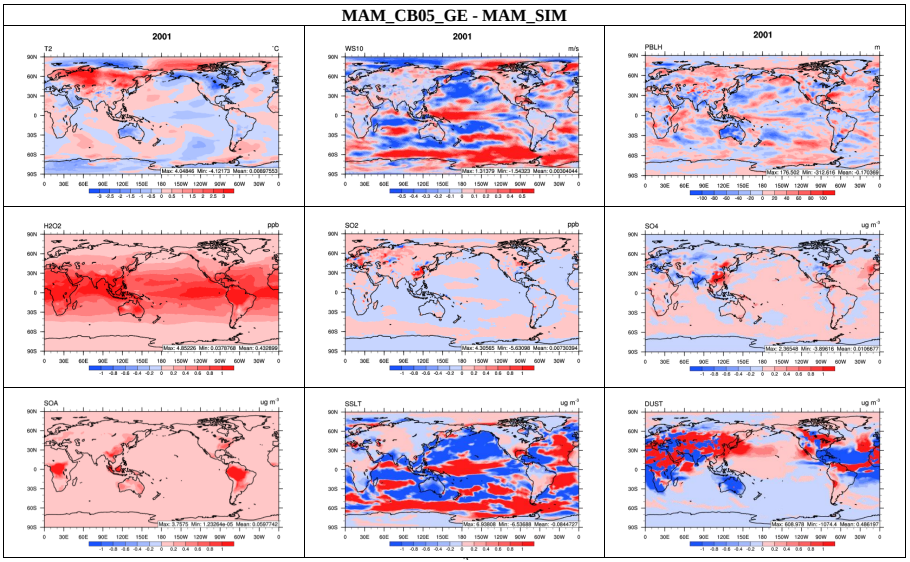

Fig. 1. Absolute differences of T2, WS10, PBLH, H_2O_2, SO_2, SO_4^{2-}, SOA, sea-salt (SSLT), and dust (DUST) between MAM_CB05_GE and MAM_SIM for 2001.

ACPD
13, 27717–27777, 2013

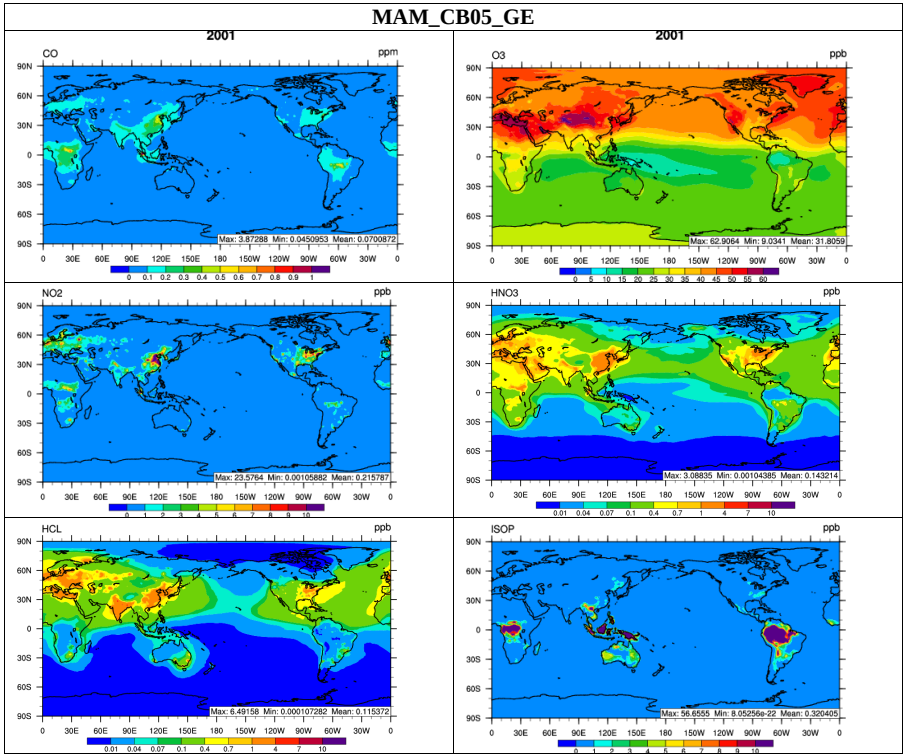

Fig. 2. Surface distribution of CO, O_3, NO_2, HNO_3, HCl, and isoprene (ISOP) in MAM_CB05_GE for 2001.

ACPD
13, 27717–27777, 2013

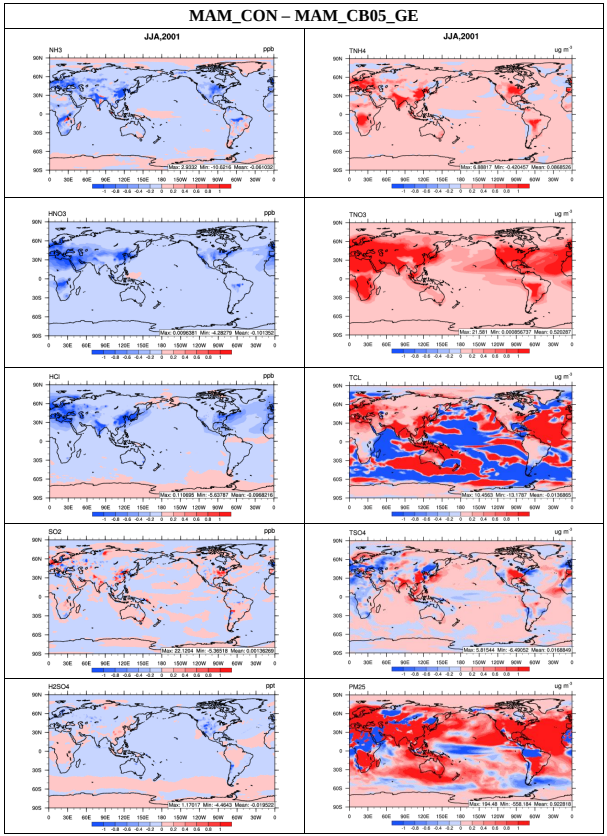

Fig. 3. Surface distribution of total ammonium, total sulfate, total nitrate, total chloride, $PM_{2.5}$, NH_3, SO_2, H_2SO_4, HNO_3, and HCl between MAM_CON and MAM_CB05_GE for summer (June, July, and August (JJA)), 2001.

ACPD
13, 27717–27777, 2013

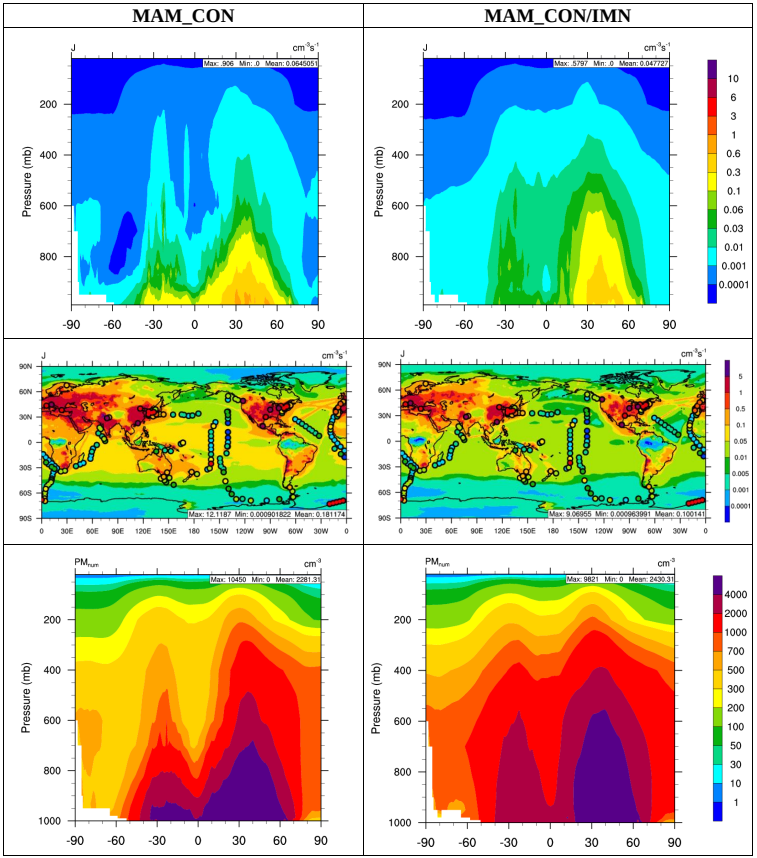

Fig. 4. Vertical distribution of new particle formation rate (J) and aerosol number (PM_{num}) simulated by MAM_CON/IMN for 2001. The overlay plots show the distribution of J in bottom 1000 m. Circles on overlay plots represent observations for J. Different colors of circles represent different values of J, using the same color scale as simulated J.

ACPD
13, 27717–27777, 2013

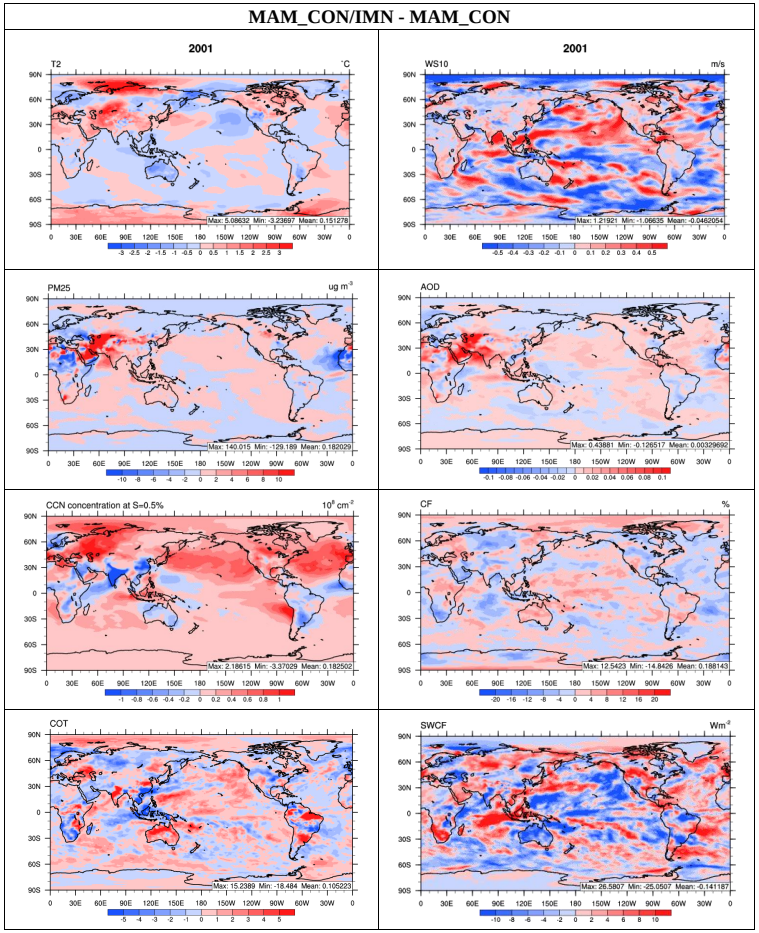

Fig. 5. Absolute differences of T2, WS10, $PM_{2.5}$, AOD, column CCN at a supersaturation of 0.5 %, CF, COT, and SWCF between MAM_CON/IMN and MAM_CON for 2001.

ACPD
13, 27717–27777, 2013

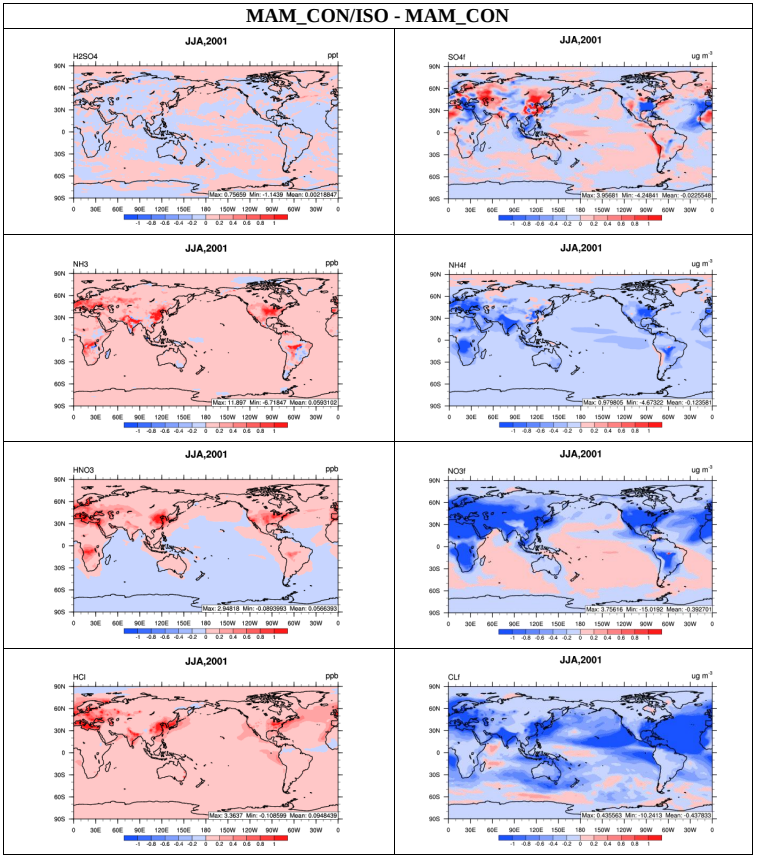

Fig. 6a. Absolute differences of major PM species and their gas precursors between MAM_CON/ISO and MAM_CON for summer, 2001.

ACPD
13, 27717–27777, 2013

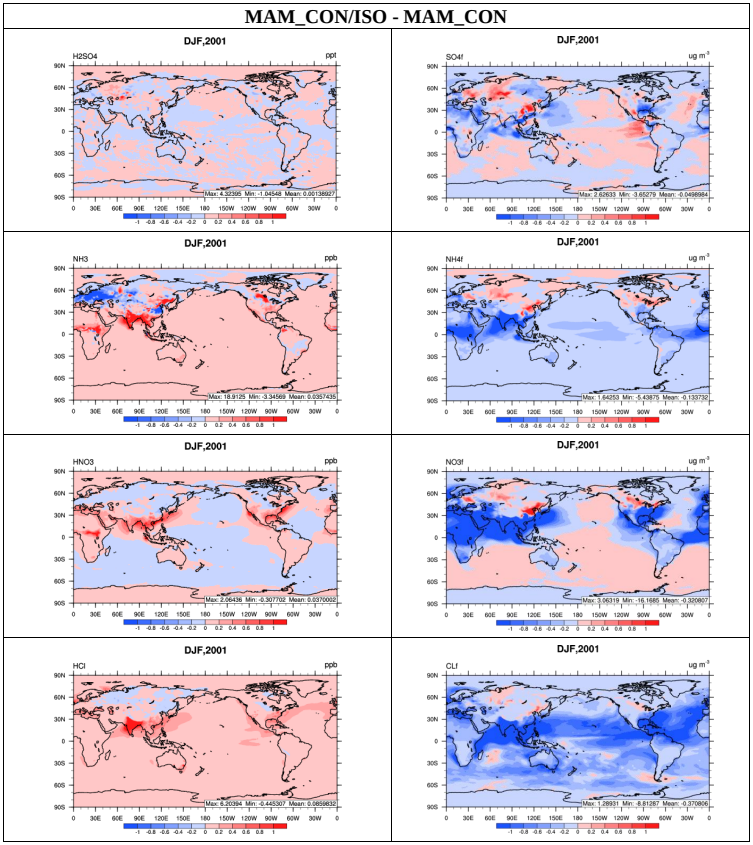

Fig. 6b. Absolute differences of major PM species and their gas precursors between MAM_CON/ISO and MAM_CON for winter, 2001.

ACPD
13, 27717–27777, 2013

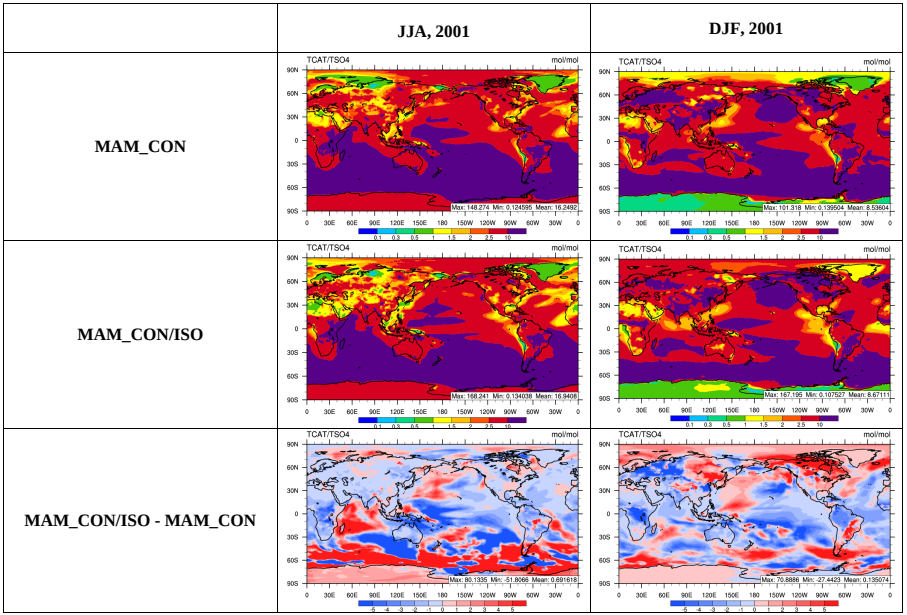

Fig. 7. Surface distribution of TCAT/TSO4 in MAM_CON and MAM_CON/ISO and absolute differences of TCAT/TSO4 between MAM_CON/ISO and MAM_CON for summer and winter, 2001.

ACPD
13, 27717–27777, 2013

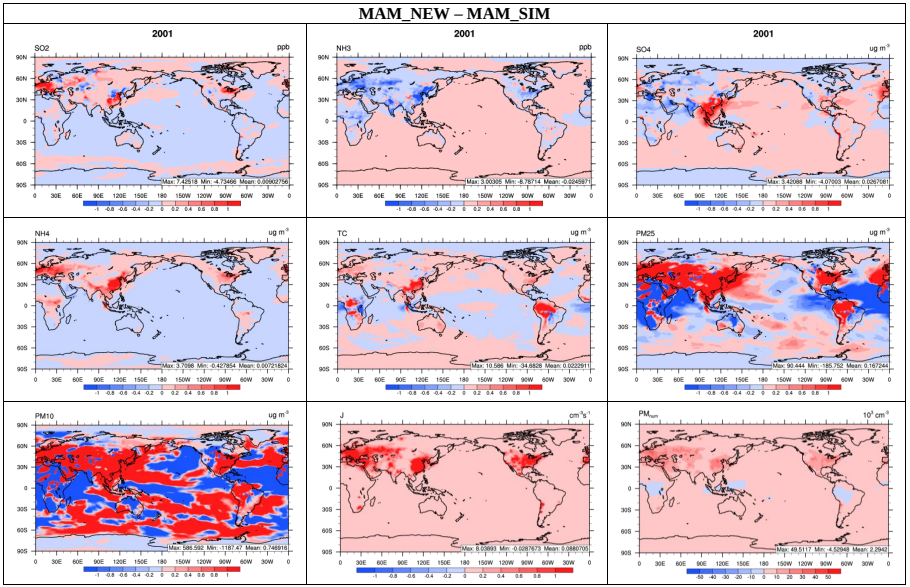

Fig. 8. Absolute differences of major aerosol species and their gas precursors, new particle formation rate, and aerosol number between MAM_NEW and MAM_SIM for 2001.

ACPD
13, 27717–27777, 2013

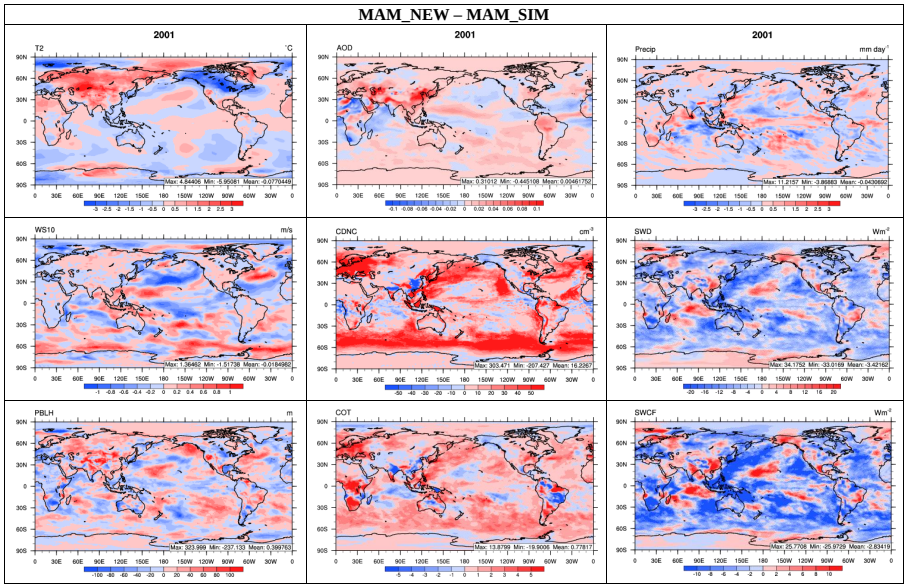

Fig. 9. Absolute differences of major meteorological variables, cloud variables, and radiative variables between MAM_NEW and MAM_SIM for 2001.

ACPD
13, 27717–27777, 2013